L3HARRIS SECONDARY MIRROR SUPPORT STRUCTURE

Joshua Nova-Yingst **Kaitlyn Bartlett** **Matthew Stead** **Angel Bermudez** **Stanley Huang**

ABSTRACT

Lattice structures are created by repeating unit cells in carefully designed and optimized patterns, allowing for weight reduction while maintaining the ability to withstand stress and loads from the environment. With advancements in additive manufacturing, the ability to produce these structures with minimal material waste and lower costs has made them increasingly valuable in the aerospace industry, where a high strength to weight ratio is essential. The goal of this project is to find out the best lattice configuration for the structure of a Secondary Mirror Support Structure (SMSS) that can be effectively fabricated with additive manufacturing in metal materials. To meet the goals of this project, the team took inspiration from last year's accomplishments to help form our initial concept designs and implement them with lattice eventually. A series of lattice, geometry, and topology optimizations were conducted to further improve our designs towards meeting the requirements and specifications. Using the designs from last year as references, our team focuses mainly on optimizing internal lattice structures in a model with a combination of different dimension meshes rather than improving the load-bearing geometry of the structure. This report will highlight the iterative design process, finite element analysis, manufacturing and testing, and supporting analysis data. These techniques and results combined to create a model that meets all the provided requirements and specifications.

PROBLEM DEFINITION

Secondary Mirror Support Structure (SMSS) is a mount used in some large telescopes for holding optical mirrors. These structures must be highly durable and require precise manufacturing methods. Increased durability and precision come at the cost of increased expenses and time, and as such, L3Harris is looking into additive metal manufacturing to potentially reduce manufacturing time while increasing production capacity.

REQUIREMENTS, SPECIFICATIONS, DELIVERABLES

REQUIREMENTS:

- The design and analysis of a SMSS model as well as a physical prototype.
- The model must be 3D-printable in titanium or invar, and it must be able to hold 23 pounds of equipment.
- The SMSS shall interface to the Forward Metering Structure (FMS) at three locations 120 degrees apart.
- The SMSS shall provide interfaces with and support the Secondary Mirror and its mounts, the Actuator Assy, the Shade Assy, and all necessary thermal hardware.
- There shall be no trapped cavities, and the entire structure must be considered "precision cleanable" by L3Harris metrics.
- The following factors of safety shall be used in analysis:
  - Yield Stress: 2.0
  - Micro-Yield Stress: 1.0
  - Ultimate Stress: 2.5
  - Buckling Stress.: 4.0
- The following mass contingency factors shall be used:
  - Concept Design: 20%
  - Preliminary Design: 15%
  - Final Design: 10%
  - Post-Final Design: 5%
  - Measured Hardware: 0.10%

TABLE 1
SPECIFCIATIONS

Description	Method of Evaluation
1. The outer diameter of the SMSS (interface to the FMS) shall be 48 inches	NX sketch of a 48-inch circle around the model
2. The first mode of the SMSS shall be 120 Hz or greater when grounded at the FMS interface and supporting all hosted hardware	NASTRAN Solution 103 Modal Analysis
3. The mass of the SMSS shall be 18 lbm or less	NX Solid Model Properties
4. The SMSS shall have positive margins of safety against yield and	NASTRAN Solution 101 Linear Statics

ultimate failure when exposed to a quasi-static load of 12 G laterally and 18 G axially simultaneously (lateral swept 15-degree increments) while supporting all hosted hardware	
5. The SMSS shall have positive margin of safety in a 5°C to 35°C temperature range while supporting all hosted hardware	NASTRAN Solution 101 Linear Statics
6. The SMSS and the hosted hardware shall not obstruct more than 14% of the Primary Mirror (PM) clear aperture area of 1.1 meters diameter	NX Solid Model Properties
7. The average motion of the SM interfaces under a 1 degree C isothermal load should be 0.66 micro-inches translation (RSS of x and y) or less	NASTRAN Solution 101 Linear Statics
8. The average motion of the SM interfaces under a 1 degree C isothermal load should be 0.037 micro-radians rotation (RSS of Rx and Ry) or less	NASTRAN Solution 101 Linear Statics

Deliverables:

- Preliminary Design Review (PDR).
- Final Design Review (FDR).
- 3D-printed scaled SMSS model.

CONCEPTS

The L3Harris team developed 3 main concept designs for the SMSS as shown in Appendix A below, with two new designs, and one being last year's model.

Design one is the final model presented by the previous team and is used as the baseline for the other 2 concepts described below. This design incorporates a circular center to reduce weight and the area of obstruction for the field of view. Also, the legs of the structure interface tangent to the circular center to combat the translation and rotation of the structure in and about X and Y axes when thermal loads. Shape optimization was performed, resulting in an adjustment to the leg lengths. Specifically, the leg lengths, measured from the mount pad to the interface of the outer and inner curvature, were refined to 1.99624 inches and 16.9962 inches, respectively. The structure is internally shelled to a thickness of 0.1 inches, without any internal lattice, and features arms that are extruded at a 38-degree draft angle from the vertical axis. Additionally, the underside walls are pointed and shelled to a thickness of 0.104 inches. For meshing, CTETRA(10) elements with a size of 0.125 inches were implemented, and the material chosen for the structure is titanium. As a result, the total weight of the model is 40.7071 lbf, yield strength of 116,755 psi, and an ultimate strength of 122,556 psi. In terms of vibration characteristics, the first vibration mode occurs at a frequency of 123.38 Hz. Furthermore, the displacement at the first positive buckling eigenvalue is recorded at 90.19, as depicted in the provided figure. Moving on to safety considerations, the lowest margin of safety based on ultimate stress, is 0.9384, while the lowest margin of safety based on yield stress is 1.5383.

Design two was designed under the concept of effectively distributing load throughout the continuously curved strut. From the single rectangular cross section with a width of 0.8” at the end of the strut where the mounting points are, it splits into two sections with 0.67” width each. The strut continues in a constant radius of curvature to merge with the other half of the other strut, forming three continuous curves. This model uses titanium alloy from the NX database. It has dodecahedron lattice with 1-inch edge length and 0.05-inch rod thickness, filling all the internal space enclosed by the outer shell with 0.1-inch shell thickness. The model has a weight of 21.4 lbm and covers 13.97% of the primary mirror area. Its vibration frequency at mode 1 is 161.53 Hz shown in Figure 13 and has a first positive buckling eigenvalue of 525.58. The lowest margin of safety happens at 12 g lateral load applied at 150 degrees from the x axis at the high temperature of 95ºF, with ultimate and yield stress allowed at 0.7 and 0.9, respectively.

Design three was made with the intention of maintaining the uniform displacement from the isothermal load while improving stiffness and increasing resistance to vibration. The design is radially symmetrical but still has the beams meet at the outer edge of the mounting points so that the forces are distributed in a similar manner to last year’s design but, in this case, the beams extend on both sides of the external mounting point (where the SMSS connects to the satellite). Like Design 2, this NX model’s material is NX’s titanium alloy and has a 0.1-inch shell thickness and a dodecahedron lattice with a 0.05-inch rod thickness and a 1-inch edge length (size of unit lattice) filling all internal space. As seen in the matrix below, the model is currently too heavy and displaces nearly double the allowed amount. The latter issue will be addressed later after running lattice optimizations and after completing the team’s lattice testing and analyzing all of the data. The weight issue will also be address via an optimization solution. It is currently 23 Lbm and covers 12.5% of the primary mirror area. Its 1st vibrational mode is 165.94 Hz and its buckling eigenvalue is 222.29 Hz. Finally, its lowest margins of safety are 2.1 for yield, and 1.8 for ultimate, both from the determined worst-case scenario which is a 12g lateral load applied at 180° from the x-axis and at the upper temperature limit of 35°C. In order to reduce the run time for the structural simulations and to take advantage of model symmetry, only 12g loads from 30-210° were used and duplicated for the high temperature and low temperature conditions. For all designs, the model has fixed constraints at each of the three external mounting points on each of the beams.

TABLE 2
PUGH MATRIX FOR CONCEPT SELECTION

	Design 1	Design 2	Design 3
Total Weight	0	-	-
Total Area	0	+	+
First Vibration Mode	0	+	+
Buckling Eigenvalue	0	+	+
Translation Displacement	0	-	-
Rotational Displacement	0	-	-
Ultimate Margin of Safety	0	-	+
Yield Margin of Safety	0	-	+
Optimizable	0	+	+
TOTAL	**0**	**-1**	**3**

MECHANICAL ANALYSIS

After establishing the initial design concepts, finite element analysis was carried out on these designs and results compared against the given specifications and requirements. To do this, the team had to first set up FEM models. The key feature that distinguished this project from previous years was the use of an internal lattice. After performing testing on coupons with internal lattice's, it was determined that the team will use a dodecahedron lattice. To set up the FEM models, a 2D mesh was applied to the design, with a set shell thickness of 0.1 inches under the CQUAD(4) mesh-type. Once the shell was made the lattice was meshed to the inner face of the shell. When a lattice is used, NX will automatically assign it to a 1D beam mesh which it calls a lattice-beam mesh. This mesh will have the same properties and dimensions as outlined in the part file and there is no way to manually create a lattice mesh so all attempts at modeling were centered around ensuring NX was able to auto-generate meshes for the lattice. Utilizing an RBE3 mesh-to-face, the lattice was meshed to the inner wall of the structure. To represent the additional 23 lbm-worth of equipment the SMSS is supposed to support, 3 Concentrated Masses were added. These were made by creating 0D meshes and placing them at the approximate center of mass of each part (this was based on locations used by previous groups from previous semesters). Each 0D mesh was assigned its appropriate mass with an additional 2/3 lbm added as the project description notes an additional 2 lbm-worth of miscellaneous equipment which was divided among the three concentrated masses. Each 0D mesh was meshed to the SMSS at the proper mounting points (indicated in the project description) using a point-to-point RBE3 connection. Reference images can be found in Appendix C, Figures 1 and 2.

This process was changed from the original design during optimization to ensure the part could properly accommodate mountings from pins and screws. The part was cut and subtracted so that only 1/6th of the original model remained. This included 1/6th of the central portion and one of the two arms that converged at each mounting point. Part of the lower surface was removed following results from topology optimizations, the results of which are in Appendix C, Figures 3 and 4. Instead of applying a 2D mesh to the 3D part, the design was closed-shelled to a final optimized design of 0.0765 inches. The results of the optimization can be found in Figure 15 in Appendix C. After this, solid blocks were added, and certain faces were moved around all the mounting points to ensure there was sufficient material to allow fasteners to properly interface with the part. The next step was to mirror and pattern the 1/6th portion radially to complete the part. This way, a solid portion of material was the interface between each 1/6th portion rather than a lattice (which created problems during simulations). After mirroring, each hollow portion which resulted from the shell was converted to an additional solid portion. From each of these solid portions, a lattice was applied and applied in a radially symmetrical manner. Each lattice portion was defined to be parallel along each of the six arms so that each 1/6th section had a lattice that was mirrored across each interface. The lattice was made to be dodecahedron, set to have a rod diameter of 0.045 inches, and given an edge length of 0.9 inches. This was based on lattice optimization simulations conducted, the results of which can be found in Figure 15 in Appendix C. Any unconnected portions of the lattice were removed. Once the lattice was applied, the interior solid bodies were suppressed, and two beams were placed across the empty space in the center of the part in order to support the mounting points that exist there (taken from previous groups). This part was then sent to an FEM and SIM, and it can be seen in Appendix C, Figure 3. Additionally, in Appendix C, are figures representing the dimensions of the design as well as the final internal structure including the optimized lattice and the modified shell.

In the FEM, the lattice (as per a built-in NX function), was automatically assigned to 6 lattice-beam collectors, one for each of the six lattice portions. Next, the outer body was assigned a CTETRA(10) 3D mesh with the element size being 0.125 inches. After this, all exterior faces of the part were grouped, all interior and exterior faces were placed in an additional group, the former was subtracted from the latter. The lattice portions were then collectively meshed-to-face to this interior-faces group using an RBE3 connection. After this, the 0D meshes were added, assigned and connected following the same process outlined earlier. The resulting FEM can be found in Appendix C, Figure 7.

Once in the simulation file, a variety of solutions and solver methods were created. All three external mounting points were set to be fixed constraints, and an array of G-loads were added to be used in different solvers. Each of these and their results are explained under the "Model Testing" Section.

MANUFACTURING

As indicated by the title of the project, the only method of manufacturing is 3D printing. The current, consumer-level 3D printing market is expensive. A 40% scale model of the final design cost roughly $450 in aluminum and $5000 in titanium. Additionally, smaller companies lack the printing resolution required for space-grade components. All of the metal-printed parts arrived late and incomplete or misshapen. Due to the printing and shipping delays, a similar version of the part was broken into four pieces and printed using the ABS 3D printers in the Rettner shop. Turnaround time from print start to finished parts was between 24 and 36 hours due to the required soak to remove infill. When it comes to potentially printing a full-size version of the part, costs must be considered. Printing the full 4-foot diameter part in the analyzed material; titanium, would cost over $450,000 and take a week to print. This is assuming no print errors. There are only a few space-flight worthy materials that this project was allowed to explore, while only titanium was used, invar and aluminum were all listed as potential candidates. Given that there was more than a 2-week delay for all parts ordered from the vendor used for this project, this timetable is likely inaccurate. After printing and shipping, a small amount of shop time is required to create all 38 holes and mounting points. It is assumed that (about 3 hours is needed for each group of holes. A rough estimate of time is tabled below.

TABLE 3
MANUFACTURING ACTION AND COST

Manufacturing Action	Cost in $
Printing Part	$450,000
Shop Time	$1000

It should be noted that because there is only a single part, no team member manufacturing time is included. The development time and cost per hour per team member is included below.

TABLE 4
TEAM COST BREAKDOWN

Team Member	Total Hours	Total Cost
Angel Bermudez	125.6	$12,560
Joshua Nova-Yingst	163.75	$16,375
Kaitlyn Bartlett	138.75	$13875
Matthew Stead	110.5	$11050
Stanley Huang	115.5	$11550

Unfortunately, there are very few printers on the market with a print bed of more than square foot. One printer was found; the EBAM 300 Series from Scaiky [1]. The company lists no price but does note their titanium printer prints at 15 lbs of material per hour. Given the finer precision and more complexe geometry of this part, it is likely that printing will take a bit longer, but it does mean that the structure could be printed in a matter of hours. If large-scale production of this part were to take place, just one of these printers working regularly could produce a dozen of these parts within a week of around-the-clock printing.

TEST PLAN AND RESULTS

Testing for this project consisted of two components, coupon testing and model testing. The overall goal of the coupon testing was to validate the true material properties of 3D printed coupons with an internal lattice as well as to find the best combination of shell thickness, edge length and rod diameter which yields the highest stiffness to weight ratio. Testing on the model is done to validate the FEA results.

COUPON TESTING

Before testing began, the team had to decide on which types of lattices to test. To determine this, NX data was used to identify the top ten lattice designs based on which lattice possessed the most desirable stiffness values, particularly in the z direction. Next, the printability of each lattice had to be analyzed based on the overhang capabilities of the campus 3D printers. Using these parameters, the list of potential lattice designs was narrowed down to three choices of Dodecahedron, BiTriangle, and Star. Although NX gave data on the stiffness of these lattices in the x, y, and z directions, it was necessary to test all lattice designs to validate NX data. Therefore, nine coupons were printed with dimensions of 7 x 1 x 1 inch in PLA with a 0.05 in shell thickness. To test the samples, four-point bend testing was chosen, with a 6-inch gap between bottom rollers, 3 inches between the top rollers and an applied load of 1100 lbf. The four-point bend testing configuration is shown in Appendix B, Figure 1.

The results of the initial four-point bend testing with the 7-inch-long coupons proved to be inconsistent, with large variances in points of failure between all three testing groups. The inconsistency in results was determined to be due to the inconsistency of the 3D printing itself, specifically the low resolution of the 3D printer. To overcome this issue, printing switched onto a higher resolution ABS 3D printer on campus.

Due to the inability to accurately print the BiTriangle lattice as well as the Star lattice failing in NX simulations due to its asymmetrical stiffness properties, the dodecahedron lattice was chosen to focus on due to its uniform stiffness in all directions as well as having the least 3D printing complications on the ABS printers. As such, the next round of four-point bend testing focused solely on the Dodecahedron lattice coupons. Three of these models were reprinted, all with the same lattice parameters (0.05-inch rod thickness and 0.5-inch edge length). The method to obtain the stiffness data from the force-displacement graphs of these coupons is shown in Figure 2 of Appendix B. The simulation of the model is shown in Figure 3 of Appendix B. The three tested coupons had an average stiffness of 2755 lbf/in and an average mass of 1.15 oz, whereas the simulated model had a stiffness of 6395 lbf/in and a mass of 2.09, as seen in Figure 4 of Appendix B. The percent error between the testing and simulated results was 56.92% for the stiffness and 44.91% for the mass.

The simulated model had stiffness and mass that were roughly double that of the tested models, which led to speculation that something in the NX model was resulting in double the stiffness. After further observation, it was determined that the simulated model was shelled twice—once during the creation of the part itself, and then again when making the 2D thin shell connection in the finite element model. Once editing the model to omit the double-shelling, the stiffness of the simulated model dropped to 3654 lbf/in, resulting in a percent error of 24.61% to the tested coupons, as seen in Figure 5 of Appendix B. Despite the improvement in the percent error, it was still too high to validate the simulation model relative to the tested models. Therefore, it was concluded that further testing needed to be conducted to determine where the discrepancy in results came from—specifically testing that focused on determining the ABS filament material properties.

It was necessary to determine the Young's Modulus (E) of the ABS filament that was being used for the 3D printed coupons—the high percent error seen between the testing and simulation results was thought to be partially due to the differing Young's Moduli values between the actual ABS filament and the ABS material properties listed in the NX database. Therefore, a test coupon modeled as a rectangular beam with reduced thickness was 3D printed and underwent the same four-point bend testing as seen in Figure 1 of Appendix B. The Young's Modulus was determined using the equation seen in Figure 6 of Appendix B [2]. Using the maximum displacement of the beam from the linear region of the force-displacement curve and the applied force at this displacement, as shown in Figure 6 of Appendix B, the Young's Modulus of ABS was determined to be 1.635e6 kPa, as shown in Figure 7 of Appendix B, which is lower than the given E value of 2.0e6 kPa in the NX database. Using this value for the Young's Modulus, the simulated 7-inch dodecahedron model's stiffness was reduced to 2981 lbf/in, with a percent difference of 7.59% between the simulation and testing stiffness values, as seen in Figure 8 of Appendix B.

Since the SMSS model is designed with titanium alloy, it was necessary to validate the testing results of a metal coupon relative to a simulated model made of the same material. Before 3D printing and testing metal coupons, it was decided that the dimensions of the coupons should be reduced to speed up the testing process, limit resource consumption, and reduce the cost required to print 3D metal coupons. As such, the ABS coupon dimensions were reduced to 4 x 0.75 x 0.75 inches, with the same dodecahedron lattice infill as 7-inch coupons. This reduction resulted in reducing the print time from 2 samples printed in 28 hours to 6 samples printed in 18 hours. A total of nine four-inch samples were printed, three of which had the dodecahedron lattice at 0.04-inch rod thickness, another three had 0.045-inch rod thickness, and the last three had 0.05-inch rod thickness. All nine models underwent the same four-point bend testing as seen in Figure 9 of Appendix B with the goal of validating the simulated results of these shorter models when compared to the testing results. The purpose of validating the four-inch ABS coupons before proceeding with the metal coupons was to ensure that the results found from simulation can accurately predict the results from physically testing the same model to then ultimately say with confidence that the 3D printed metal SMSS with lattice will behave as the simulations predicted.

While reducing the coupons' dimensions significantly sped up the manufacturing process, these shorter samples had local failure rather than global failure during the four-point bend testing, which led to much higher percent errors in the average stiffnesses, ranging from 54.8% to 56.0%, as seen in Figure 10 of Appendix B. The local failure was attributed to the bottom and top supports of the four-point bend test to be too close to each other, resulting in internal shearing of the beam instead of bending when the test was conducted. Since the simulation of the four-inch models could not be validated when compared to the real models due to such high percent errors between the results, the testing method was switched to a three-point bend test to allow for greater room between the top and bottom supports, as seen in Figure 11 of Appendix B.

Three-point bend testing was conducted on six four-inch samples with dodecahedron lattice infill, three of which had 0.07-inch rod thickness and the other three had 0.06-inch rod thickness. These rod thicknesses were utilized after determining that the stiffness-to-weight ratio seemed to increase with larger rod diameter of the lattice. All samples had 0.65-inch edge length between each lattice unit—this edge length was also utilized after seeing a pattern in which the stiffness-to-weight ratio increased when increasing the edge length. The 3D printed samples with 0.06-inch rod thickness had an average stiffness of 2975.6 lbf/in, and the 0.07-inch rod thickness samples had an average stiffness of 3116.5 lbf/in. The 0.06-inch and 0.07-inch rod thickness simulated models had stiffnesses of 3055.6 lbf/in and 3098.6 lbf/in, respectively. The NX simulation of the 0.07-inch rod thickness model is seen in Figure 12 of Appendix B for clarification on how the stiffness was calculated from the maximum displacement. Therefore, the percent error between the tested coupons and simulated models were 2.62% for the 0.06-inch rod thickness model and 0.58% for the 0.07-inch rod thickness model, as seen in Figure 13 of Appendix B. These percent errors were sufficiently low enough to conclude the three-point bend testing with four-inch models will yield results that align with those from an NX simulation of the same testing procedure with the same model.

After validating the three-point bend testing with the four-inch ABS coupons, aluminum coupons of the same dimensions were ordered and purchased from CraftCloud. The metal coupons were supposed to have the dodecahedron lattice infill with a 0.07-inch rod thickness and 0.65-inch edge length that was seen to have the highest stiffness-to-weight ratio when compared to the lattice parameters. Upon arrival, it was seen that the models lacked the lattice infill and were only shelled, but there was discrepancy in the dimensions—the sides of the models were sloped, leading to variable thickness and width of the models. For instance, sample 1 had 0.05-inch shell thickness on three sides except for one side being 0.06 inches, and the thickness of the shell for sample 3 ranged from 0.044 inches to 0.066 inches. The aluminum samples are shown in Figure 14 of Appendix B, and microscopic images of the cross sections highlight the variable shell thickness, which are shown in Figure 15 of Appendix B.

Despite the missing lattice in the metal coupons, three-point bend testing was still conducted to see how well the simulated test correlated to the testing performed on the MTS machine. To model the metal coupons in NX, the shell thickness measurements of the metal samples were averaged, and these averages were used as the shell thicknesses in the simulated models of each sample. The simulation is shown in Figure 16 of Appendix B. Despite efforts to align the simulated models to the samples, the percent errors between the masses were relatively high, ranging from 22.2% to 23.2% as seen in Figure 17 of Appendix B. Additionally, the percent errors between the simulated and testing stiffness values was also a bit high, ranging from 2.98% to 10% as seen in Figure 17 of Appendix B. The discrepancy between the simulated and testing results can likely be attributed to the high variability in the metal coupons' dimensions as well as the coupons being constituted of numerous elements. Upon completion of mass spectroscopy analysis, the samples were seen to be only 80% aluminum by weight, with carbon and silicon comprising the next largest mass percents of 7.83% and 7.63% respectively, as seen in Figure 18 of Appendix B. The NX simulations modeled the metal coupons as being made solely of aluminum, and as such, the Young's Modulus and other material properties utilized in the simulations were different than the actual material properties of the coupons, therefore leading to the differences seen between the simulated and tested samples' masses and stiffnesses.

To validate our final, optimized structure, a model needed to be obtained and tested as with the coupons. Unfortunately, the price to print a 4-foot structure in ABS was over $17,000 and over $450,000 if titanium was to be used so a scaled model had to be made. A 40% scale model was determined to be small enough to fit on low-level consumer-grade printers but to be printable, the model had to be modified. It was decided to print the part from Craftcloud and out of the same aluminum as the test coupons. The lattice was changed to a star lattice as it had a small enough overhang angle to be compatible with the specific Craftcloud vendor. Additionally, because their minimum wall thickness remained 1 mm, the shell and lattice thicknesses had to be adjusted. The arms were changed to be completely solid and the rest of the shell was increased to 1 mm. The lattice was also changed to be 1 mm thick and was now only present in the center. Unfortunately, as with the test coupons, this part was delayed in printing and did not arrive in time to test. So, a variation of the scale model was made, replacing the star lattice with the original dodecahedron lattice and was printed using the school ABS printers in 4 parts. Each leg was printed separately and re-attached with 24-hour epoxy. This was held in place during drying with plastic sheeting and restrained with clamps to ensure a secure bonding between the pieces.

To test the validity of all the simulations conducted, this scaled model was tested twice, in two different setups and a comparable model was made in NX using the scaled model file that was printed. This model did not use the NX values for ABS but instead used the calculated value, found from coupon testing. The first test was a free-free vibration or an unconstrained solution 103. These setups are in Appendix A, Figure 19. The resulting 1st mode from this solution was 87.09 Hz. It is very difficult to create a truly free-floating, real-world part for vibrational testing, but it was approximated using bungies suspending the model at each of the three legs. An accelerometer was placed on the part, and a special hammer connected to the Siemens vibration software was lightly tapped 5 times next to the accelerometer. The resulting data (Appendix A, Figure 20) was then analyzed and found to produce a 1st mode of 90.89 Hz. This presented a 4.36% difference between a tested and simulated result, indicating that the models used would perform similarly if real-world versions were made. To confirm this confidence, another test and simulation was made, to measure stiffness. The real model was placed on a granite block used to determine flatness and, specifically, the ends of the three arms were placed on rollers. A small platform was placed in the center of the model and a displacement gauge was put at point on the part. The setup is shown in Appendix A, Figure 21. A 50-gram mass was placed on this platform and the displacement was measured. The measured displacement was 2.45E-03 inches, yielding a stiffness of 44.98 lbf/in. A similar model was set up in NX using the same load and measuring displacement from the same point. The calculated displacement was 2.398E-03 inches and so, meant a stiffness of 45.995 lbf/in. This meant a –2.207% difference between the simulated and tested models. These similarities indicate a high degree of confidence in the full-scale, optimized, final design.

MODEL ANALYSIS

There was a significant amount of model analysis conducted. This included developing and testing the preliminary model, developing, setting up and running various optimization simulations, repeatedly conducting non-simulated optimizations, setting up and running new model iteration analysis, result and data verification analysis and finally, specification verification analysis. It should be noted that for all solutions, an additional parameter, AUTOMPC was always turned on due to the inclusion of a lattice.

Beginning with initial model verification as well as final model verification, both models were given the same loads, constraints and used the same solutions and solving methods. It was these results that were compared to the given specifications to determine how the part stacked up. The first solution was Solution 103 Real Eigenvalues, which was used to test the modes of vibration. The solution was simple and only required the fixed constraints at each of the three external mounting points. The requirements stated that the 1st mode must be at least 120 Hz. The initial model had a 1st mode of 165.94 Hz, and the final model had a 1st mode of 120.12 Hz. Both of these meet the requirement. The second solution was a Solution 101 Linear Statics solution and was used to test the 1-degree Celsius isothermal displacement. An initial temperature of 5 degrees was set with an added load of 6 degrees. The physical constraints were also included. The allowed displacement was 6.6E-7 inches translational and 3.7E-8 inches rotational which was to be measured from the 0D mesh representing the secondary mirror. NX reports the values in each axis, so an RSS was done on the values given by it. The initial model had a translational displacement of 8.97E-7 inches and a rotational displacement of 6.54E-8 inches. The final model's results were 9.3E-6 inches translationally and 5.347E-7 inches rotationally. After the isothermal solution, another Solution 101 was set up to test the G-loads and temperature range. An initial temperature of 68F was set and temperature loads of 5C and 35C were each added. Next an 18 G vertical load was added (in the positive z-axis because the part was extruded upside down). Next 12 G loads were applied laterally in the center of the part at 15 degree increments so that a lateral G-load in any direction could be approximated. This solution was run and, afterwards, all of the loads were distributed into combined loads. Each load contained the 18 G load, a lateral G load and a high or low temperature. This way, for each lateral load, there would be a vertical load and a high and low temperature version. These results are not included as the specific stresses were not to be reported, however visuals of the simulated models can be found in Appendix C, Figure 8. The combined loads were then placed into Margin of Safety solver, and it was from here that meaningful data was extracted.

For the initial model, two margins of safety were set up, one to test the ultimate MS and one for the yield MS. The maximum ultimate and yield values were taken from the NX materials database for titanium alloy at 37 degrees C. These values are 361630 kPa for the former and 317986 kPa for the latter. Additionally, only the 2D elements were selected as locations from where to report the margins of safety. The specifications allow for any positive margin of safety when a factor of safety of 2 for ultimate, 2.5 for yield and 4 for buckling are taken into account. The resulting MS values are 2.1 for ultimate and 1.8 for yield. Based on these results, and a 12.5% primary mirror coverage, it can be said that all requirements and specifications were met by the preliminary design except for three; the secondary mirror displaces too much in a 1C isothermal load, it weights 5 lbs more than the 18 lbm allowed, and the part has none of the required equipment interfaces.

The final model saw its MS values solved slightly differently and had additional results. The same loads and combined loads were taken from the 101 solutions but, different and more accurate allowable stress values were selected. Because the values reported by NX varied with temperature, even over the small range of temperature we were given, it was decided that a low temperature and high temperature margin of safety would be calculated for each allowable stress. For the ultimate margin of safety, the low temperature allowable value was 414750 kPa while the high temperature value was 400171.5 kPa after incorporating an FS of 2. The yield allowable low temperature value after using an FS of 2.5 was 304600 kPa and the high temperature value was 291621 kPa. While the differences between these values are only ~3% the difference was enough to see separately reported MS values based on temperature. All the results can be found in Appendix, but the lowest MS value found was 0.4823. This value came from the 12G, 5C, 105 degrees from x-axis load. This value was from the 3D elements only. When the 1D (lattice) elements were included in the margin of safety calculation, the resulting value dropped to -0.5998. This result indicates that the lattice fails well before the overall structure does and that the overall structure still has a positive margin of safety. The location of every lowest MS is in Figure 17, Appendix C. This load was then taken and used in a buckling solution which yielded an eigenvalue of 149.49 with a lattice and 81.19 without. This, in turn, meant a buckling MS of –0.991 without a lattice and –0.997 with one. From all these results, it was determined that, overall, 2 of the requirements and specifications were not met. Again, the secondary mirror concentrated mass displaces too much under the isothermal load and there is a negative buckling margo The cross-sectional area of the final design was not measured because, from the point of view of a potential primary mirror, no external geometry was changed. All changes were made to the internal geometry and to external geometry in the z-axis only so, the coverage of the PM remains 12.5%. On a additional qualitative piece of data found in Figure 16 of Appendix C, shows the comparison of the first vibrational mode, and the lowest MS failure mode. Clearly, they move (and will likely fail) in the same way, displacing primarily along the z-axis. As expected, this part is weakest to forces, loads and stresses in the z-axis, more so, than other directions.

In between the analysis of the initial and final designs, a series of optimization studies were conducted to improve the geometry of the part and determine accuracy of the analysis being conducted. The first of these analyses was the shell and lattice optimization.

The lattice and shell optimization began by taking the preliminary model, removing the two crossbeams in the center of the structure and then using datums to cut the part into to six radially symmetrical pieces. All but one was removed. The results of this first 1/6th model and simulation iteration as well as the resulting mirrored part and simulation are in Appendix C, Figures 10 and 11. The first simulation conducted was a simple load applied to a 23 lbm 0D mesh in the center of the part and mounted at the center and corner of each of the six interior faces. The magnitude of displacement of the concentrated mass in the center was then measured and compared as was the visualization of part deformation. The 1/6th model's maximum displacement was 3.112e-04 inches while the full part's maximum displacement was 3.062E-04 inches. The difference between these two values is small enough to be considered negligible and, as can be seen in Figures 10 and 11, the shape and coloration of displacement are nearly identical across the two parts. Once the 1/6th set up was validated, a series of optimizations were run. The goal was to reduce weight while limiting displacement to the specifications given. With these limitations, the Solution 200 Optimization solver was to check a variety of values for the lattice rod thickness and the shell thickness, ranging from, at first, 0.01 to 0.2 inches. The load used for these simulations was, at first, the 1C isothermal temperature load (run in the full part only) which can be found in Appendix C, Figure 12. The resulting optimum lattice and shell thickness was found to be 0.01 inches for both metrics. Because the low end of the range was found to be optimum, the simulation was rerun, this time, with no lattice exported to the solver. These results are in Appendix C, Figure 13. Again, a 0.01-inch-thick shell was found to be optimized. This proved that these variables had no effect on displacement from the isothermal load, indicating that the displacement was actually affected almost completely by the shape and geometry of the part.

The next optimization was another Solution 200 but this time, using the same load as previous, 46119 psi. The range of values for the lattice thickness were changed to 0.045 to 0.1 inches and the range of the shell was changed to 0.045 to 0.2 inches. The company that was to be used to print a metal version of the final design had a maximum wall thickness listed at 1 mm or approximately 0.045 inches. As seen in Appendix C, Figure 15, the weight was reduced by about 15% and the final lattice thickness was found to be the minimum of 0.045 inches while the shell thickness was reduced to 0.0765 inches. This simulation proved to be quite intensive, took over 2.5 hours and ended up damaging the SSD the simulation was running on. It was later discovered that the SSD in question was too slow for the processor on the computer so, in the future, when running any optimization or other intensive simulations, it is recommended to use a supercomputer such as BlueHive if access can be gained, or to use school computers. Due to the hardware issues, no visuals of the simulation could be acquired and so cannot be displayed. This was the final lattice and shell optimization run.

The other optimization simulations were topology analyses, with the goal of altering the part geometry to better support the required loads with the least amount of material. Two separate topology optimization studies were conducted to evaluate material distribution and improve the structural efficiency of the model under an applied load of 18G. The first study, titled Max Stress Limit, constrained the design based on 80% of the Titanium Alloy's yield strength, prioritizing structural performance under stress (Appendix C, Figure 3). The second study, Max Mass Limit, limited the final part mass to 18 lbm, focusing on weight reduction while maintaining load-bearing capability (Appendix C, Figure 4). Both studies applied shape constraints to prevent overhanging geometry and enforce repeated rotational symmetry, with construction bodies fixed at both ends and the load applied centrally. Based on these results, the decision was made to remove material along the top face of the model, which significantly reduced overall weight while preserving critical load paths.

Several additional non-optimization studies were conducted. The first was a trial-and-error test on the two beams in the center of the part. When comparing the SM displacements from the isothermal load (visuals in Appendix C, Figure 18) it appears that the two crossbeams in the center of the part expand under the thermal load and push the middle section apart. Because these two beams break the radial symmetry of the part, this causes the secondary mirror to displace rotationally and translationally and displace beyond the allowed limit. To address this, different actuator mount orientations were simulated. The results are in Figure 19 of Appendix C and are also tabulated below.

TABLE 5
GEOMETRY STUDY OF THE CENTER

	Translation (in)	Rotation (rad)	Weight (lbm)
Original	9.3e-6	5.347e-7	16.93145
2 Beams	5.158e-6	1.659e-7	17.30182
4 Beams	8.13e-6	5.4e-7	17.35347
Removed Center	4.99e-6	4.288e-7	16.96233

From this table, it seems that different geometries did lead to some minor improvement in the final design. However, most of these values remain a magnitude too high and increase the weight a noticeable amount. Due to time constraints, none of these iterations were tested for their vibrational mode nor their performance under G-loads. It is unknown if these iterations improved upon or fell short of the other requirements and specifications for this project.

A final set of simulations were designed to determine the loss of stiffness when the lattice fails and efficacy of a lattice on this particular geometry. A simple 1 lbf load was added to a new Solution 101 and was applied to the 0D mesh representing the secondary mirror. The simulation was then run twice, once with and once without the lattice. The displacements of the secondary mirror were then measured. The load was divided by these measurements to determine the difference in the structure stiffness and how much stiffness the current lattice provides and to determine how much stiffness is lost when the lattice fails (as stated earlier, it was discovered that the lattice will fail well before the rest of the structure fails). The difference in stiffness between a lattice and no lattice was found to be 530.25 lbf/in. When compared to the magnitude of the individual stiffnesses found of ~43000 lbf/in, this number seems almost negligible. Additionally, with no lattice, the 1st vibrational mode increases slightly from 120.12 to 120.2 Hz. These results indicate that the lattice, in this design, is little more than a dead weight. Figure 20 in Appendix C provides more support for this idea, as it shows two margins of safety calculations with all of the same variables. The only difference is that one has a lattice, and one does not. The difference between the two is 0.87%. The MS with no lattice was only slightly lower indicating that the addition of the lattice is negligible when it comes to structural performance. It was still believed that the lattice should improve stiffness but, because the lattice in this model was so thin, it failed before it could provide any decent improvement. To test this theory, two additional simulations were run, with a lattice thickness of 0.1 inches and 0.4 inches. No other variables were changed nor was any geometry. Additionally, the weights of all four iterations were collected so that their stiffness-to-weight could be compared. The results are tabulated below.

TABLE 6
STIFFNESS TO WEIGHT LATTICE STUDY

Thickness	Stiffness (lbf/in)	Weight (lbm)	S/W
No Lattice	43252.6	16.26	2665.75
0.045 inch	43782.8	16.93	2585.9
0.1 Inch	45787.5	19.59	2337.12
0.4 Inch	59417.7	96.68	852.77

From these results, the theory that increased lattice thickness could lead to increased stiffness is correct. The thicker lattices produce noticeably higher stiffness values. They are also much heavier and so drastically reduce the S/W ratio of the part. It is possible that other lattices, with different parameters and different orientations on different geometries could lead to different results, however, for this design, and these lattice parameters, the lattice does not improve stiffness of the part. The one thing it does improve on is printability. The internal structure means the part can be easily printed without the need to overhang–compatible geometry or removable internal supports.

TABLE 7
ANALYSIS VERIFYING ALL REQUIREMENTS AND SPECIFICATIONS

Requirements and Specifications	Verification
1. The outer diameter of the SMSS (interface to the FMS) shall be 48 inches	All geometry is contained within 48-inch diameter circle. PASSED
2. The first mode of the SMSS shall be 120 Hz or greater when grounded at the FMS interface and supporting all hosted hardware	The 1st mode of vibration is 120.12 Hz PASSED
3. The mass of the SMSS shall be 18 lbm or less	The mass is 16.9 lbm PASSED
4. The SMSS shall have positive margins of safety against yield and ultimate failure when exposed to a quasi-static load of 12 G laterally and 18 G axially simultaneously (lateral swept 15-degree increments) while supporting all hosted hardware	The lowest MS of the shell is 0.48 and the lattice MS is –0.59 PASSED
5. The SMSS shall have positive margin of safety in a 5°C to 35°C temperature range while supporting all hosted hardware	The above MS used the temperature range PASSED
6. The SMSS and the hosted hardware shall not obstruct more than 14% of the Primary Mirror (PM) clear aperture area of 1.1 meters diameter	The SMSS has 12.5% coverage PASSED
7. The average motion of the SM interfaces under a 1 degree C isothermal load should be 0.66 micro-inches translation (RSS of x and y) or less	Average motion is 9.3 micro-inches FAILED
8. The average motion of the SM interfaces under a 1 degree C isothermal load should be 0.037 micro-radians rotation (RSS of Rx and Ry) or less	Average motion is 0.54 micro-radians FAILED

INTELLECTUAL PROPERTY

The final geometry of the team's design of the Secondary Mirror Support Structure (SMSS) is patentable due to its originality and the novel methods used in its development. In comparison to previous years, the design is unique in relation to shape, side profile dimensions, and the integration of an internal lattice structure. Earlier teams such as the 2024 L3Harris Team also utilized topology optimization, however, their design was more constrained by the overhang limitations, often resulting in excess material being used to overcome this (Appendix D, Figure 1). In contrast, the 2025 team's design embraces greater geometric freedom due to the lattice yielding improved printability.

In industry, companies such as Lockheed Martin and Boeing hold patents for SMSS designs that they created. For instance, Boeing uses a more traditional arrangement with straight supports, with minimal vertical height, as seen in Figure 2 of Appendix D [3]. Lockheed Martin's design uses a network of thin rods as seen in Figure 3 of Appendix D [4]. Neither company uses lattices. In contrast, the 2025 L3Harris team's design features arms that act as cantilever beams, with thickness varying with length. The differences in the team's design compared to designs in industry are significant, with the team's design using different shapes, materials, processes, and internal design, making the design original, novel, and unique.

SOCIETAL AND ENVIRONMENTAL IMPLICATIONS

The move towards 3D metal printing for aerospace purposes such as the Secondary Mirror Support Structure, offers important benefits to both the environment and society. Typically, additive manufacturing offers faster production, more complex geometries and reduced waste when compared to traditional machining methods, which often have high wastage. Metal 3D printing does however produce around 100-500 kg of CO2 per kilogram of finished part, while composite lay-up produces 20-50kg of CO2 per kilogram, raising potential ethical and public safety concerns. Although 3D printing has a much higher C02 output, it does lead to reduced material wastage. When using 3D printing, the manufacturing process is far quicker than that of composite lay-up, with less labour, and more unsupervised production. 3D printers can manufacture parts almost 24/7, making the manufacturing process have reduced lead times, and cost.

For this project specifically, PLA and ABS test coupons were printed, which are typically not recycled due to the complex processes required. PLA must be recycled separately from other plastics due its lower melting point risking contamination with other plastics [5], and it currently does not meet the American Society for Testing and Materials (ASTM) standards of biodegradability in soil, marine, and fresh water [6]. Titanium 3D printing is recyclable, with used parts being able to be melted down and reused, a significant improvement compared to the current materials used, however many satellites never get a chance to be recycled. Although the environmental impact was higher, the benefits in cost, material efficiency and production scalability have been achieved. In the future, further optimization of parts using additive manufacturing could lead to lighter parts, reducing fuel consumption to deploy the satellites into space. Developments with 3D printing technology may help to reduce the CO2 emissions of manufacturing, reducing the overall carbon footprint of deployment.

Improving access to satellite technology through faster and cheaper manufacturing will have positive impacts on global public health. The wide spread of satellite technology enhances communication networks, supports natural disaster response systems and enables better environment monitoring. Although the manufacturing of parts, and increased fuel from satellite launches raises ethical concerns, the long-term benefits of satellite deployment are significant. Satellite systems help improve worldwide access to space-based technologies, further supporting education, development and emergency services in remote areas.

RECOMMENDATIONS FOR FUTURE WORK

Based on the results of this project, several recommendations can be made for future groups. While incorporating lattice structures may increase overall stiffness, the stiffness-to-weight ratio achieved in this specific application did not justify their use. Therefore, it is recommended that future teams carefully evaluate the trade-off between added stiffness and additional weight or complexity before implementing lattice designs.

When selecting a 3D printing vendor, it is highly recommended to begin communication early in the design process. Engaging with vendors early allows for an improved understanding of print-specific requirements such as infill density, build orientation, lead times, and potential limitations based on machine type or material. Future teams should prioritize vendors that offer detailed technical information on their websites—such as build volume, machine models, material specifications, and printing tolerances—as this information is essential for validating that the vendor can meet the demands of the design in a timely manner.

Another area of focus can be optimizing the actuator mounting beams. While the overall design demonstrated effectiveness, the actuator mounting beams of the SMSS failed to meet the requirements stated in Table 7, which impacted the overall success of the design. Future iterations should focus on refining the geometry of this area and may benefit from conducting simulations and testing specifically targeting the center.

Lastly, building on the work done by the 2024 L3Harris team is recommended, as their model successfully met all requirements and specifications. Their design incorporated peak-like features to remain within the 45-degree overhang constraint required for effective 3D printing without support structures. While this approach improved printability, it introduced additional geometric complexity that may not be necessary. Further iterations could explore alternative design modifications that maintain printability while simplifying the geometry and improving cleanability.

ACKNOWLEDGMENTS

The 2025 L3Harris Team extends appreciation to Patrick Ellsworth, Patrick Zinter, Steve Sutton, and L3Harris for their sponsorship, valuable feedback, and guidance throughout the duration of the project. The team would also like to acknowledge Professor Christopher Muir for teaching the team the necessary skills to complete the project. The team would also like to acknowledge the efforts of Christine Pratt for the numerous MTS machine testing sessions as well as analyzing the metal coupons via mass spectrometry. Lastly, the team would like to thank Jim Alkins for his support in 3D printing the test coupons as well as the plastic scaled SMSS model. All contributions were vital to the completion of the project, and the team is deeply grateful for the efforts of all involved.

REFERENCES

[1] Cruson, D., "Intuitive Machines lands on the Moon using Sciaky Ebam-made part," Sciaky [Online]. Available: https://www.sciaky.com/largest-metal-3d-printer-available.
[2] Sim, S., 2016, "Mach-1 – Extraction of Mechanical Parameters Following Bending Test." [Online]. Available: https://www.biomomentum.com.
[3] Basu, S. (n.d.). US20050088734A1 – Autonomously Assembled Space Telescope. Google Patents. USPTO report retrieved April 27 2025, from https://patents.google.com/patent/US20050088734A1.

[4] Duncan, A. L., Kendrick, R. L., & Sigler, R. D. (n.d.). US5905591A - Multi-Aperture Imaging System. Google Patents. USPTO report retrieved April 27, 2025, from https://patents.google.com/patent/US5905591A.
[5] "PLA Recycling: Everything You Need to Know." 3DEVO [Online]. Available: https://www.3devo.com/blog/pla-recycling-everything-you-need-to-know.
[6] Matsumoto, Ken'ichiro. "Enzymatic Degradation of PLA: Future Perspectives." *Poly(lactic) acid: synthesis, structures, properties, process, applications, and end of life*. Hoboken, New Jersey (2022): pp. 65-93.
.

APPENDIX A – DESIGN CONCEPTS

Figure 1. Design 1. This design is taken from 2024 L3Harris Team and was considered for further optimization as it met all specifications and requirements.

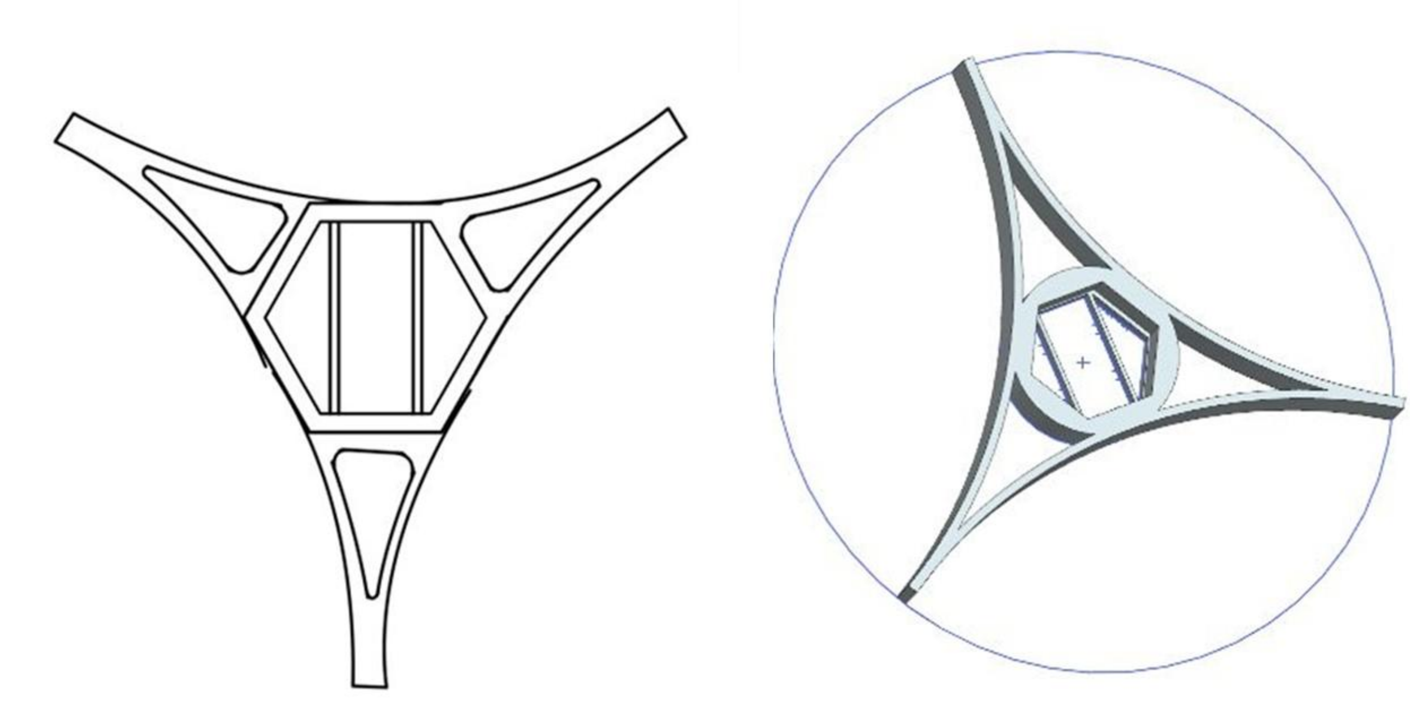

Figure 2. Design 2. This design was not chosen to be further optimized as Design 3 met more requirements and specifications, as seen in the Pugh Matrix.

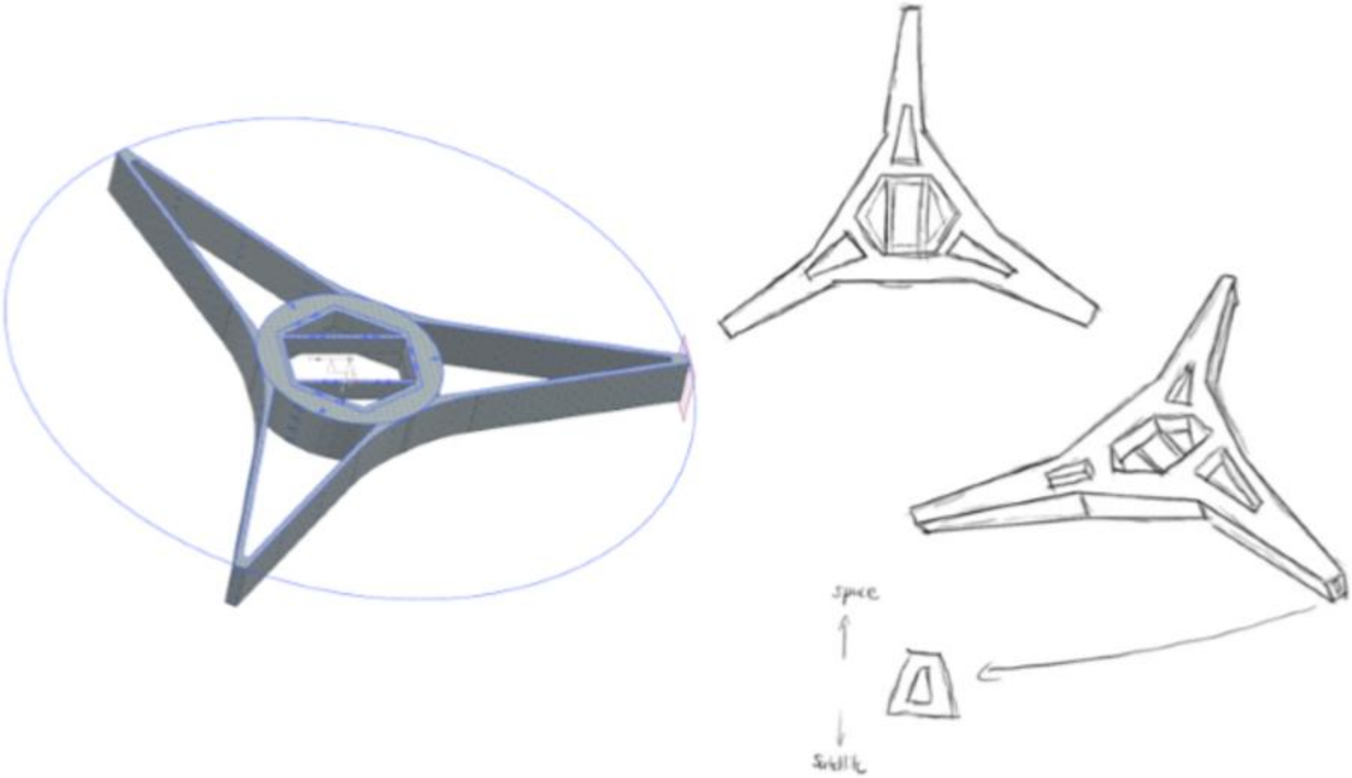

Figure 3. Design 3. This is the design the team chose to optimize further.

APPENDIX B – COUPON TESTING

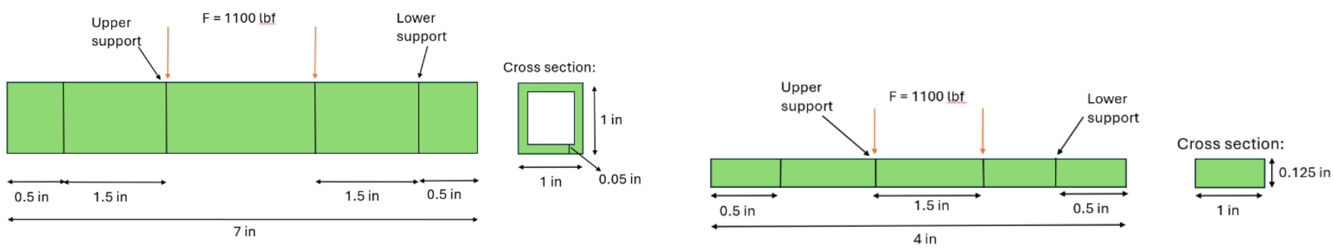

Figure 1. Visual representation of four-point bend test for the lattice infilled 7-inch models (left) and the solid test coupon (right). The 7-inch models have a shell thickness of 0.05 inches.

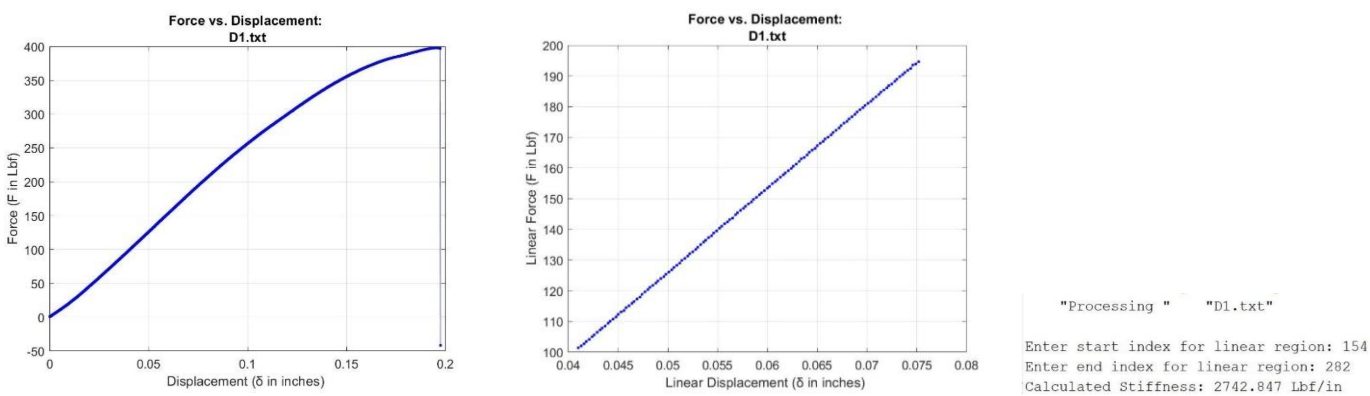

Figure 2. Force vs. displacement graph for the first dodecahedron sample (left) and the linear region (middle) from which the stiffness was calculated (right).

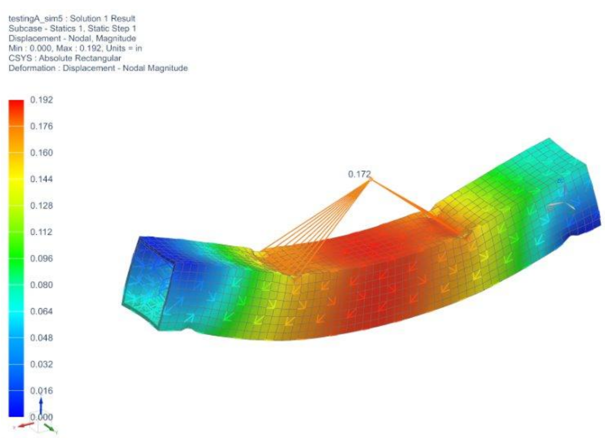

Figure 3. Simulation of the preliminary 7-inch dodecahedron model with 0.05-inch rod thickness and 0.5-inch edge length. The maximum displacement was determined to be 0.172 inches, which is the displacement of the simulated crosshead of the MTS machine.

Sample Tested	Stiffness (Lbf/in)	Mass (oz)
D1	2742.847	1.18
D2	2732.643	1.136
D3	2788.843	1.138
Average from Samples	2755	1.15
Simulated Sample	6395	2.09
Percent Error	**56.92%**	**44.91%**

Figure 4. Results the four-point bend testing with the three 7-inch dodecahedron lattice coupons as compared to the simulation results of the same model.

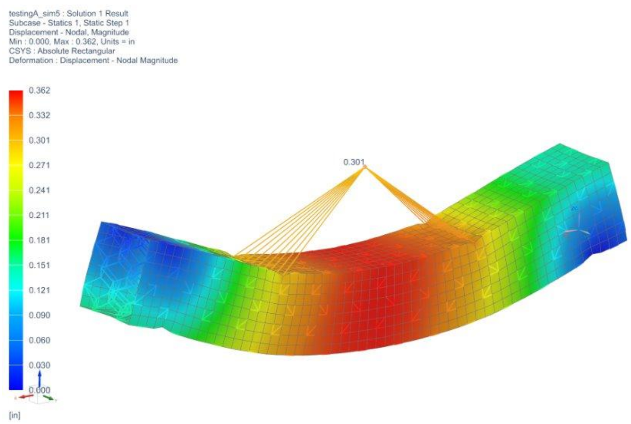

Sample Tested	Stiffness (Lbf/in)
D1	2742.847
D2	2732.643
D3	2788.843
Average Stiffness from Samples	2755
Stiffness of Simulated Sample	3654
Percent Error	**24.61%**

Figure 5. NX simulation of the 7-inch dodecahedron lattice model with only the 0.05-inch thin shell in the FEM (left), and the results table comparing the stiffnesses of the tested models to the improved simulation model (right). The percent error in the stiffness was seen to decrease to 24.61% after removing the double shell.

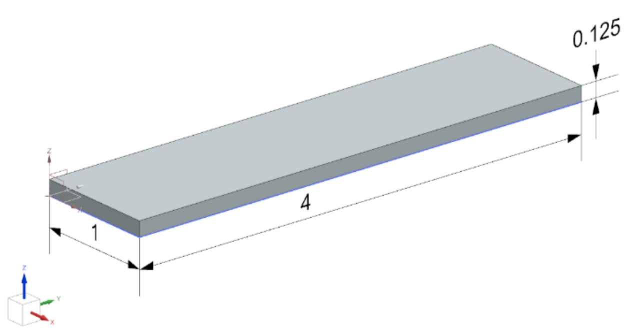

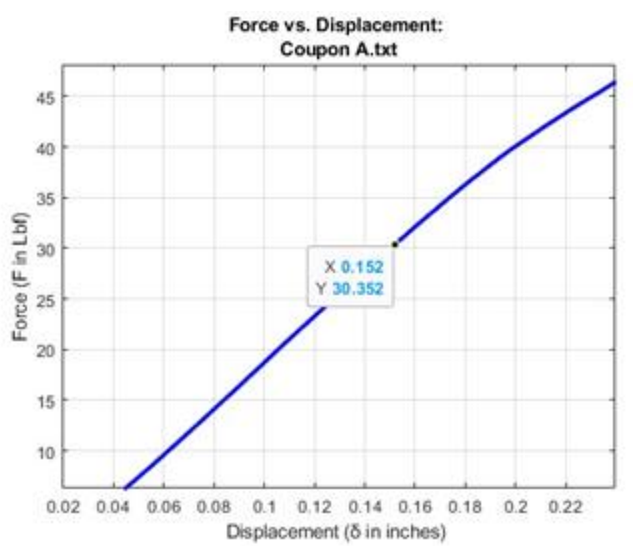

Figure 6. Force vs. Displacement Curve for ABS Test Coupon (left) and CAD model of coupon (right). The maximum displacement of the linear region was found to be 0.152 inches, and the corresponding force was 30.352 lbf. These values were used to calculate the Young's Modulus of ABS.

$$E_f = \frac{F}{\delta} \cdot \frac{L_1\left(3{L_{total}}^2 - 4{L_1}^2\right)}{48I}$$

Where

F = applied external load
L_{total} = span length or distance between the supporting pins
L_1 =distance between the supporting pin and the loading pin
δ = deformation
I = polar moment of inertia

```
%% Calculating Youngs Modulus from Test Coupon
b = 1; % width of beam, in inches
h = 1/8; % height of beam, in inches
I = (b*(h^3))/12; % polar moment of inertia

L1 = 0.75; % length between top and bottom supports
L2 = 1.5; % length between the two top supports
Ltotal = 3; % length between the two bottom supports
delta = 0.152; % max displacement of linear region, in inches
F = 30.352/2; % half of the applied forcem, in lbf, corresponding to delta

num = F*L1*(3*(Ltotal^2) - 4*(L1^2));
den = 48*delta*I;
E_english = num/den;  % resulting E in lbf/in^2 (English units)

E_Pa = E_english*6894.76; % convert psi to Pa
E_kPa = E_Pa/1000; % E in kPa
display(E_kPa)
```

Command Window

```
E_kPa =

   1.6356e+06
```

Figure 7. Equation utilized to calculate Young's Modulus for a rectangular solid beam undergoing four-point bend testing [1] (left) and MATLAB calculation of the resulting Young's Modulus (right).

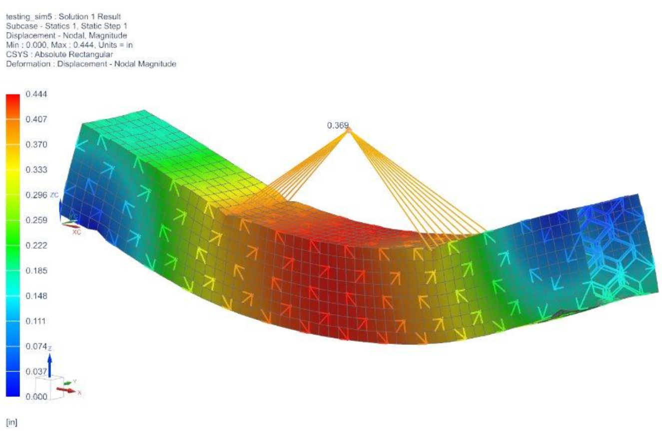

Sample Tested	Stiffness (Lbf/in)	Mass (oz)
D1	2742.847	1.18
D2	2732.643	1.136
D3	2788.843	1.138
Average from Samples	2755	1.15
Simulated Sample	2981	1.31
Percent Error	**7.59%**	**12.11%**

Figure 8. NX simulation of the 7-inch dodecahedron lattice model with the 0.05-inch thin shell in the FEM as well as the 1.635e6 kPa Young's Modulus (left), and the results table comparing the stiffnesses of the tested models to the improved simulation model (right). The percent error in the stiffness was seen to decrease to 7.59% with the reduced Young's Modulus.

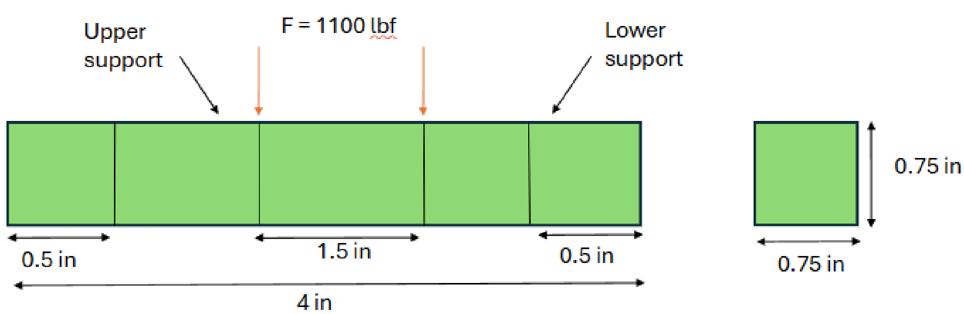

Figure 9. Visual representation of the four-point bend testing setup with the four-inch models with a shell thickness of 0.05 inches and the dodecahedron lattice inside.

Sample Tested	Mass (oz)	Stiffness (Lbf/in)
1 - 0.05"	0.403	5557
2 - 0.04"	0.384	5394
3 - 0.045"	0.398	5464

Sample Simulated	Mass (oz)	Stiffness (Lbf/in)	Percent Error in Stiffness	Percent Error in Mass
1 - 0.05"	0.454	12360	55.22%	11.23%
2 - 0.04"	0.421	12263	56.01%	8.79%
3 - 0.045"	0.436	12304	54.84%	8.72%

Figure 10. Results of the four-point bend testing with the four-inch ABS coupons. The coupons all had a shell thickness of 0.05 inches with dodecahedron lattice of 0.65-inch edge length and varying rod thickness seen in the figure. The stiffnesses and masses of the tested samples are averaged from all three coupons of sample type.

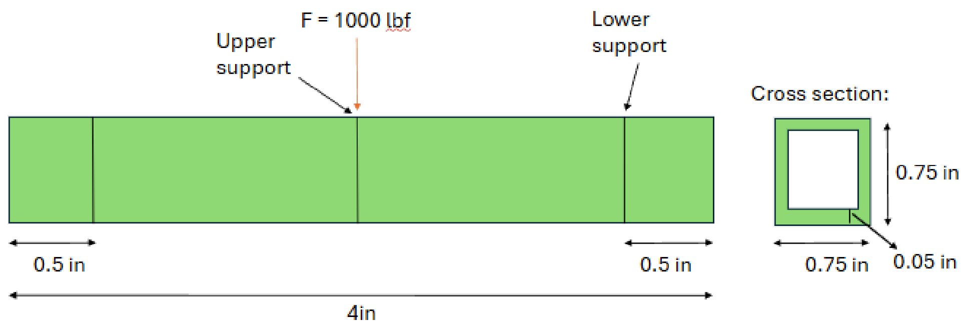

Figure 11. Visual representation of the three-point bend testing setup. The lattice infill is not shown.

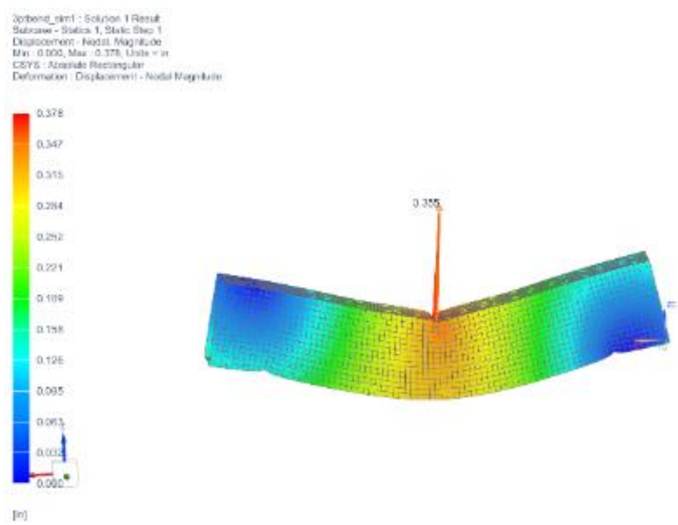

Figure 12. Simulation of the four-inch model with the 0.07-inch rod thickness dodecahedron lattice undergoing three-point bend testing. The maximum displacement was seen to be 0.355 inches, resulting in a stiffness of k = 1100 lbf/0.355 in = 3098.6 lbf/in. The 2D mesh element size was reduced to 0.05 inches to ensure all lattice components were captured.

Sample Tested	Stiffness (Lbf/in)
1A (0.06")	2992.345
1B (0.06")	2974.664
1C (0.06")	2959.791
0.06" - Average	2975.6
0.06" - Simulated	3055.56
Percent Error	2.62%

Sample Tested	Stiffness (Lbf/in)
2A (0.07")	3141.882
2B (0.07")	3096.352
2C (0.07")	3111.22
0.07" - Average	3116.5
0.07" - Simulated	3098.59
Percent Error	0.58%

Figure 13. Results of the three-point bend testing with the four-inch ABS coupons. The coupons all had shell thickness of 0.05 inches with dodecahedron lattice of 0.65-inch edge length and either 0.06-inch or 0.07-inch rod thicknesses for the lattice.

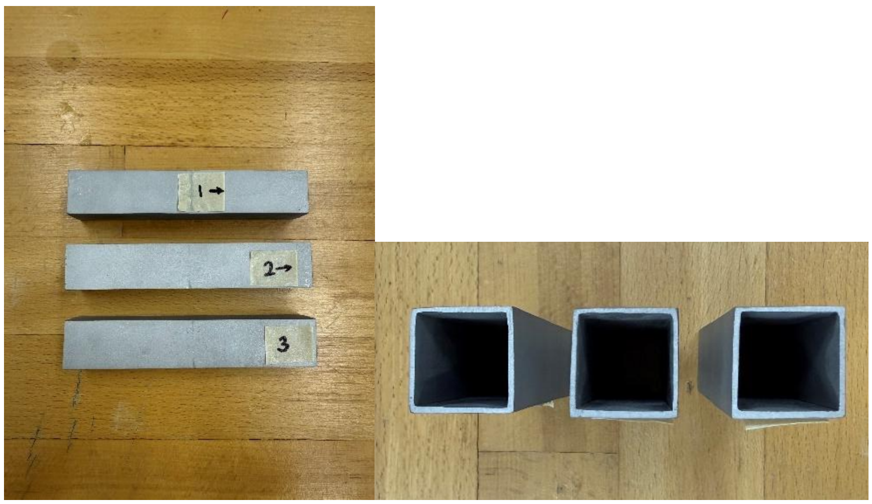

Figure 14. Side-view of the three aluminum coupons (left) and view of the cross-sectional area (right). As seen from the cross-sectional view, there is no lattice present.

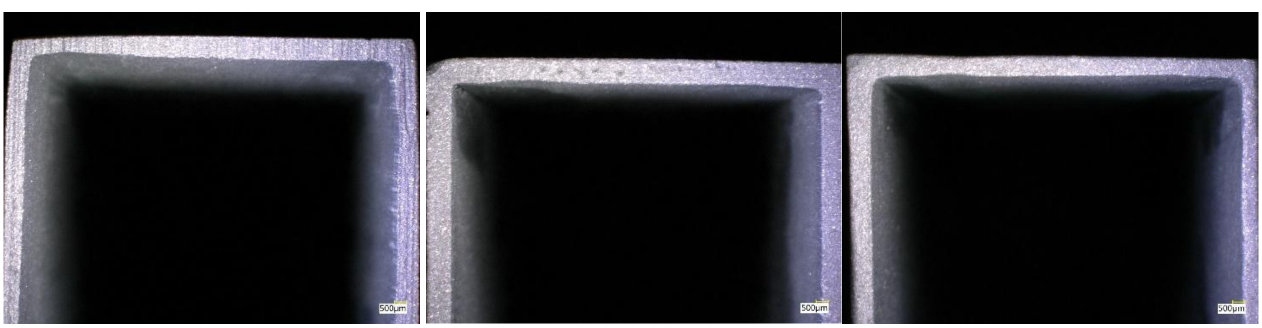

Figure 15. Microscopic images at 20x magnification of the cross sections of aluminum coupon sample 1 (left), sample 2 (middle), and sample 3 (right). The shell thicknesses vary greatly along the width of the coupons, and there are significant grooves in the metal.

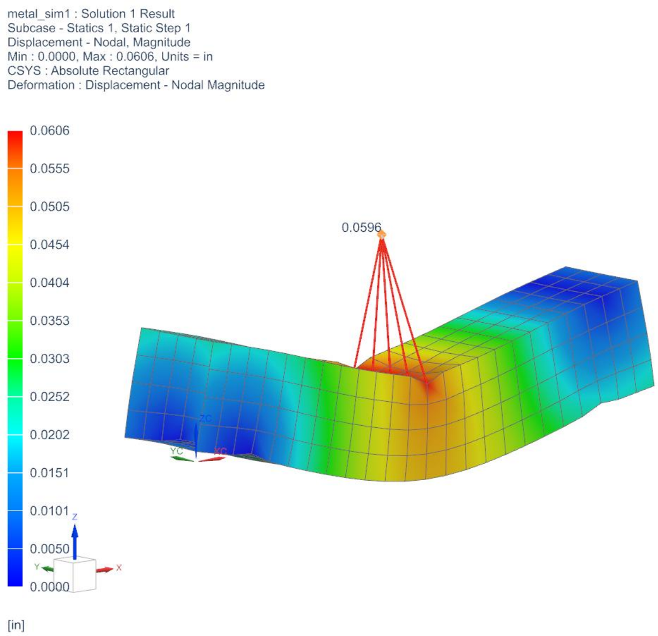

Figure 16. Three-point bend testing simulation for metal coupons. For the 2D thin shell mesh, the recommended element size of 0.193 inches was used for all models.

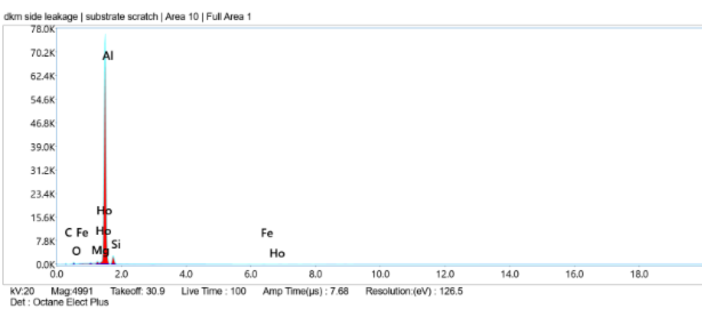

Element	Weight %	Atomic %	Error %	Net Int.	R	A	F
C K	7.83	15.82	14.20	14.85	0.8875	0.0229	1.0000
O K	3.00	4.54	12.42	34.71	0.8993	0.1102	1.0000
Mg K	0.94	0.94	6.49	65.31	0.9172	0.6566	1.0471
Al K	80.00	71.94	3.66	5552.49	0.9211	0.7432	1.0026
Si K	7.63	6.59	8.67	216.82	0.9248	0.3159	1.0020
Fe K	0.25	0.11	35.17	4.71	0.9607	0.9617	1.0695
Ho L	0.35	0.05	48.29	2.65	0.9668	0.9730	1.0207

Figure 17. Mass spectroscopy analysis of the aluminum coupons (left) with a tabulation of the % by weight of elements constituting the samples (right).

Testing Samples	Mass (oz)	Maximum Displacement (in)	Stiffness (Lbf/in)
1	0.764	0.0588	1.63E+04
2	0.778	0.0509	1.89E+04
3	0.803	0.0484	1.98E+04

Sample Simulated	Mass (oz)	Maximum Displacement (in)	Stiffness (Lbf/in)
1	0.982	0.0596	1.68E+04
2	1.013	0.0578	1.73E+04
3	1.035	0.0556	1.80E+04

Sample	Mass Percent Error	Stiffness Percent Error
1	22.20%	2.98%
2	23.20%	9.25%
3	22.40%	10%

Figure 18. Results of the three-point bend testing of the metal coupons as well as the results of the same testing simulated in NX. The stiffness percent errors were seen to be lower than the mass percent errors.

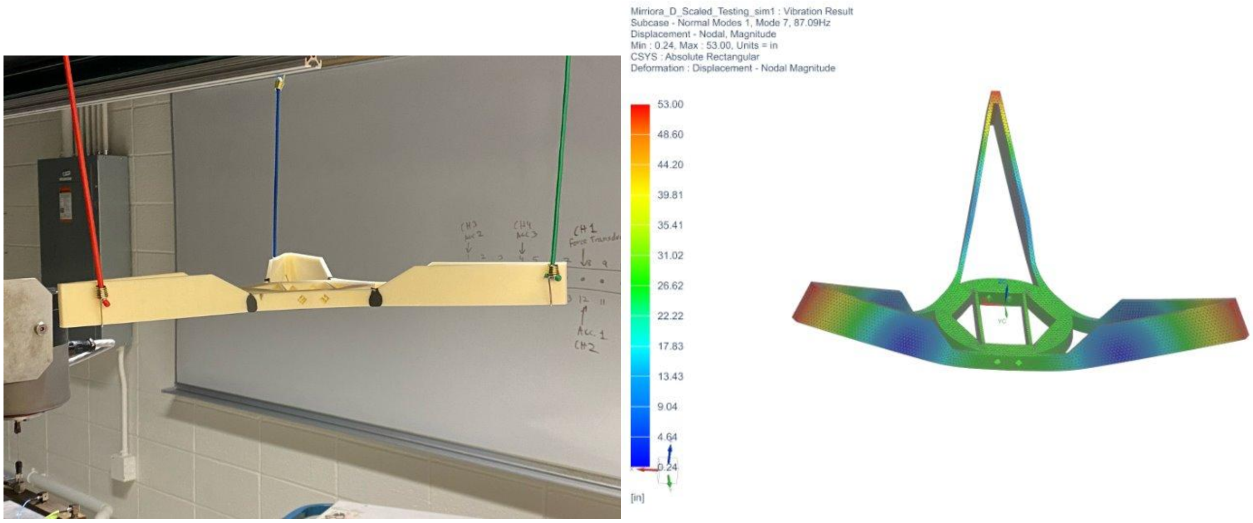

Figure 19. Model in the vibration setup and related NX vibration simulation.

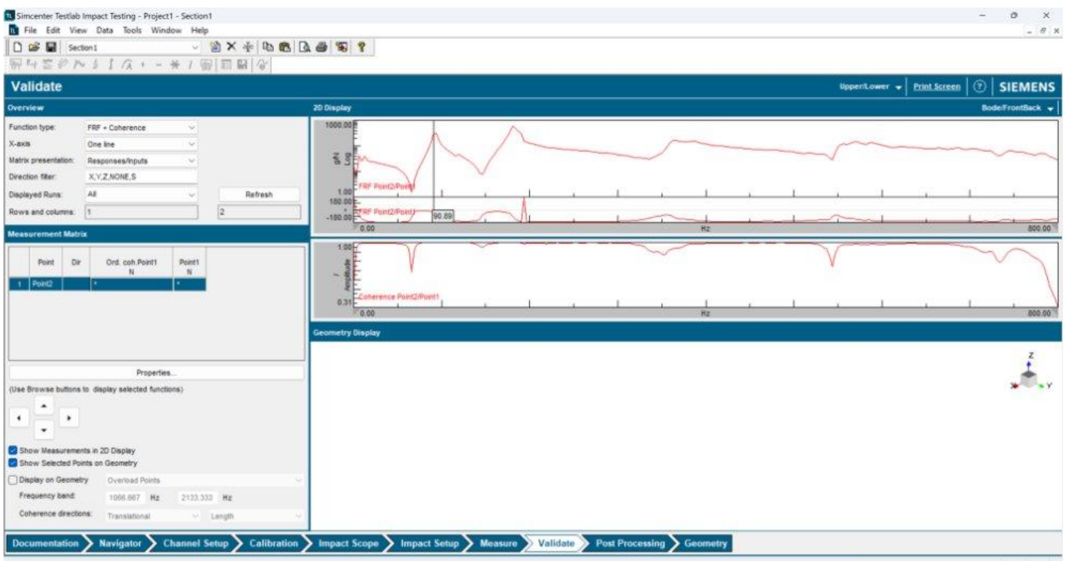

Figure 20. Tested vibrational results with peak 1st mode of 90.89 Hz.

Figure 21. Setup and measuring of stiffness of ABS printed, scale model.

APPENDIX C – MODEL TESTING AND OPTIMIZATION

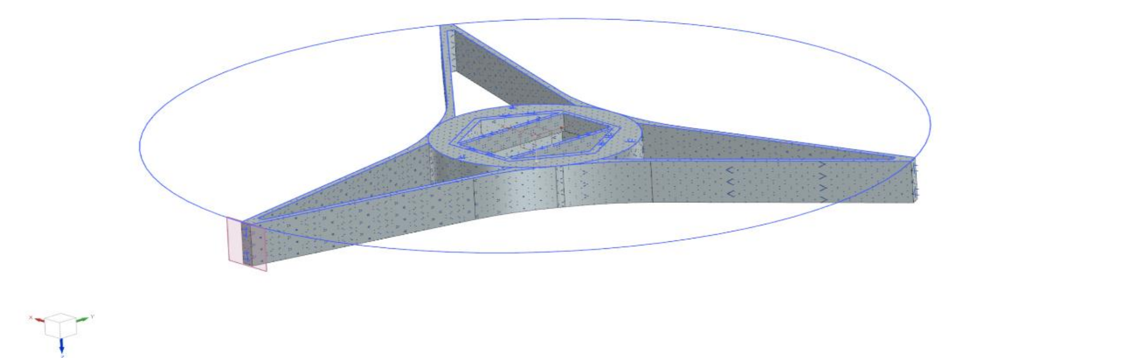

Figure 1. Preliminary design part file.

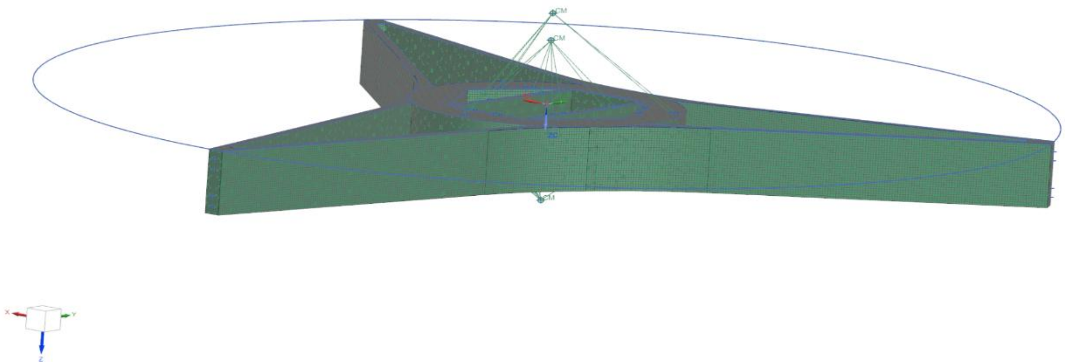

Figure 2. FEM and SIM representation of preliminary design including 0D meshes.

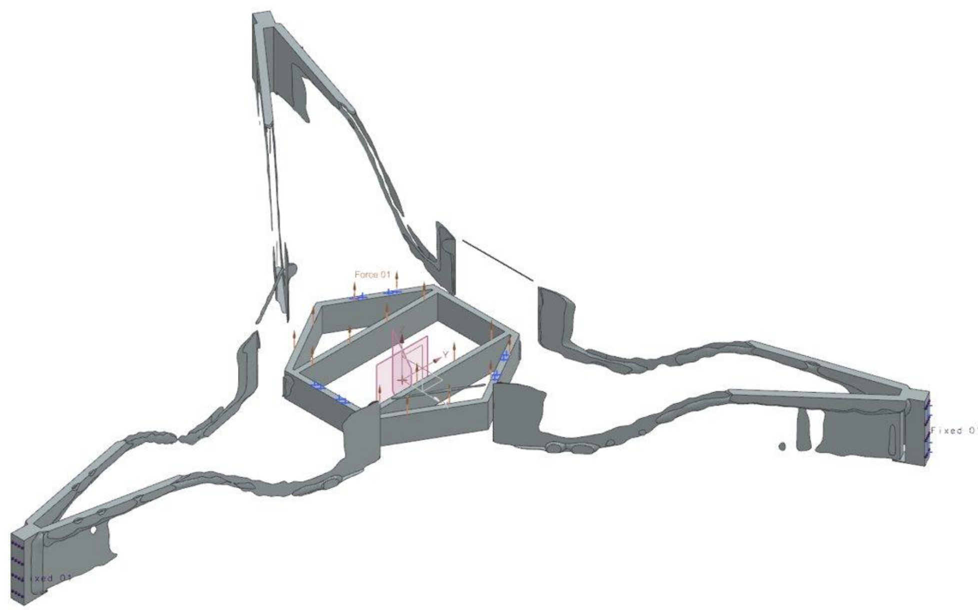

Figure 3. Topology optimizations result for the "Max Stress Limit" study.

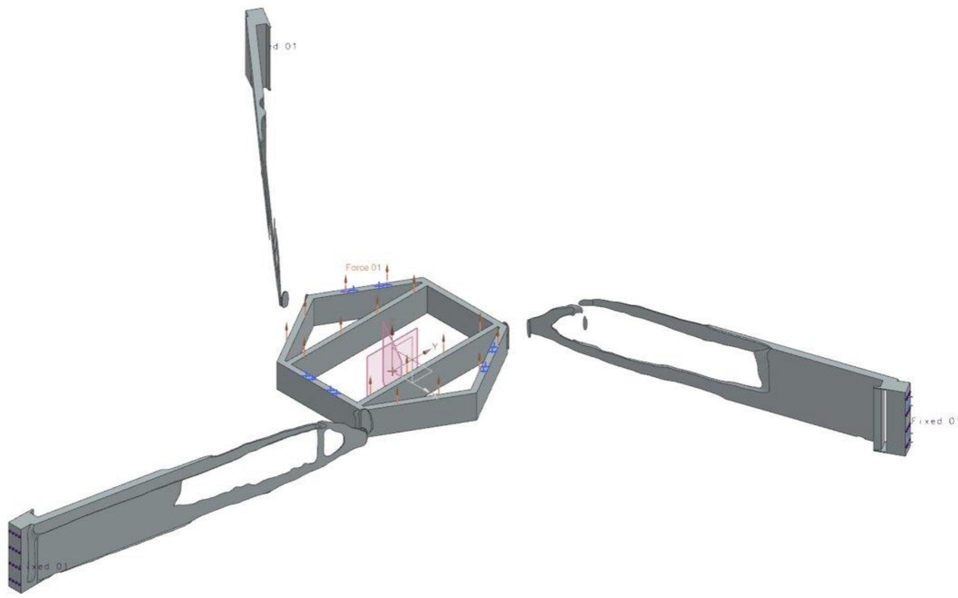

Figure 4. Topology optimizations result for the "Max Mass Limit" study.

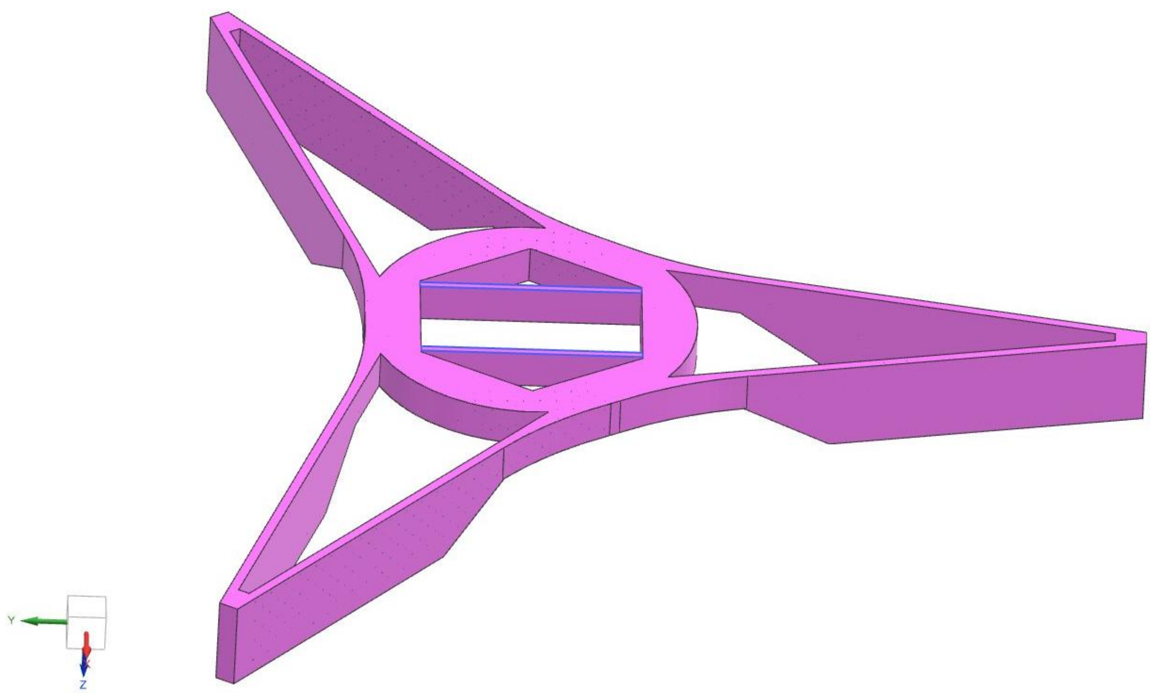

Figure 5. Final iteration of design including optimized shell and lattice and containing proper material for fasteners.

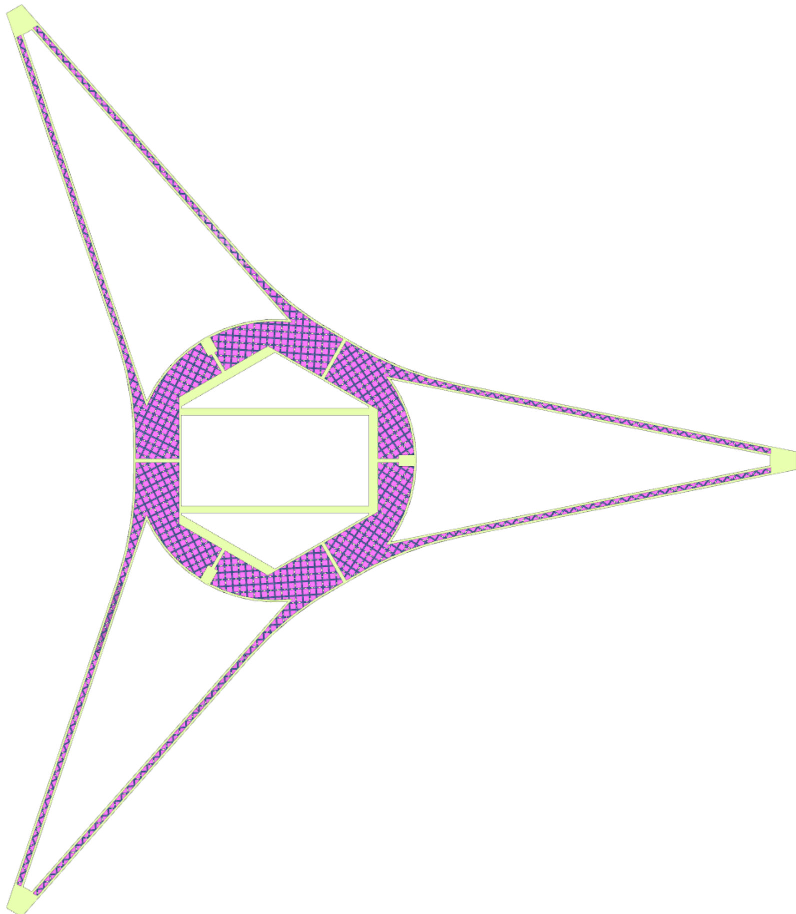

Figure 6. Cross-sectional view of final part showing lattice orientation and mounting points. The yellow sections are solid, the blue is the lattice, and the pink is the inner shell surface.

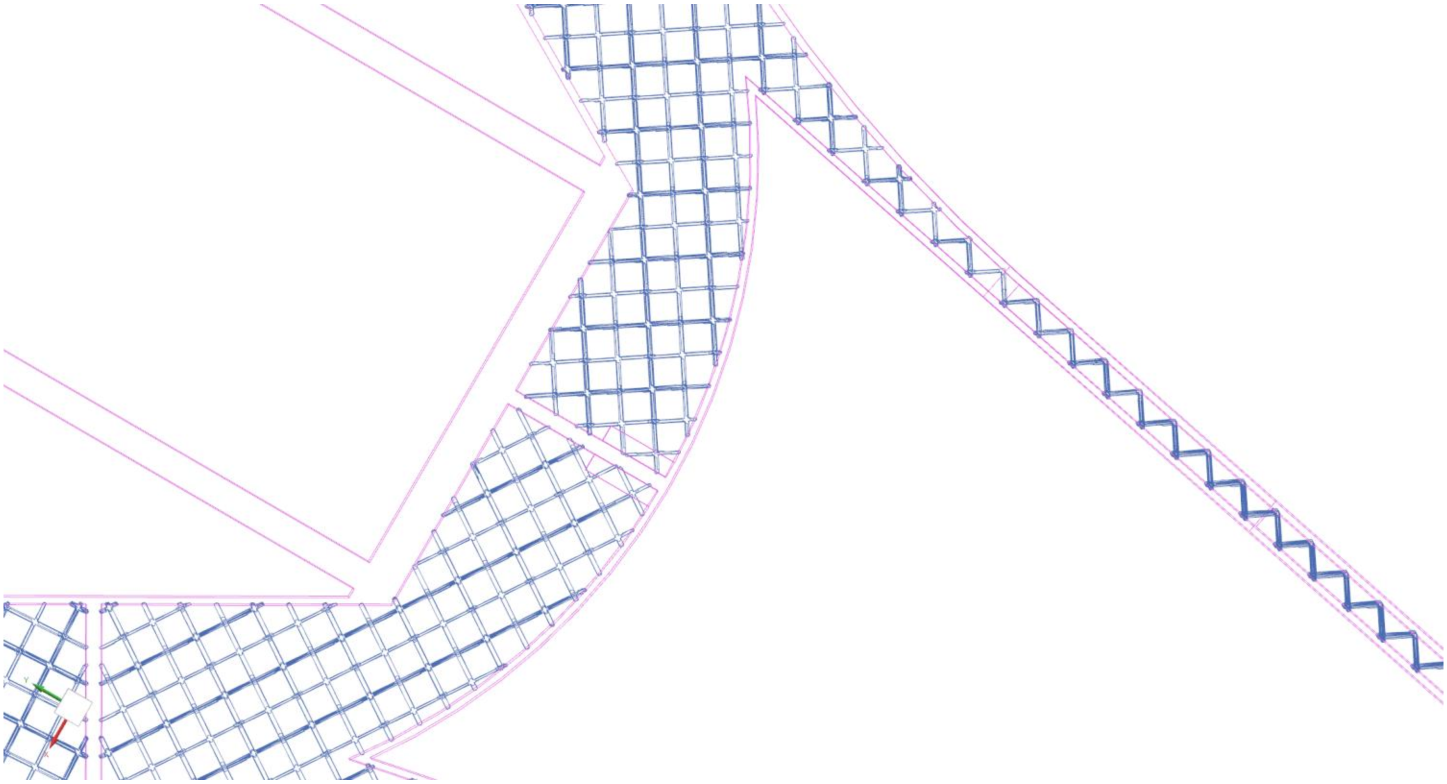

Figure 7. Wireframe view of part showing the full internal structure and providing additional views of added material for mounting. The inner border of the center varies in thickness to accommodate the mirror mounting points and the shade mounting points are accommodated by a small block on the top of the structure directly opposite the thicker border sections.

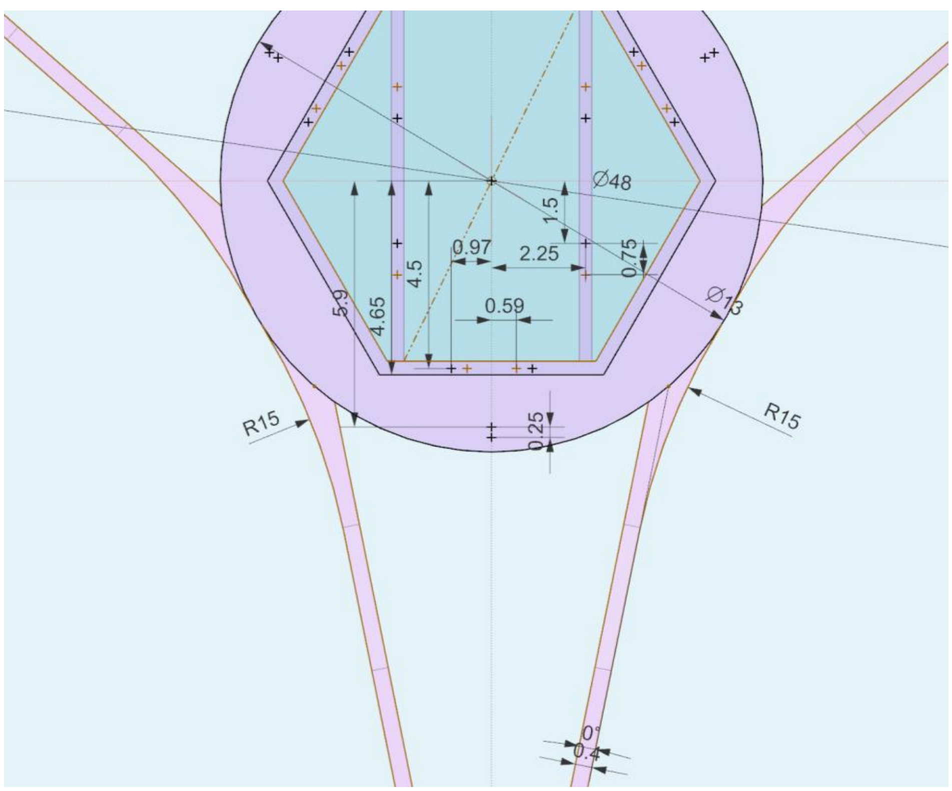

Figure 8. Dimensions of final design.

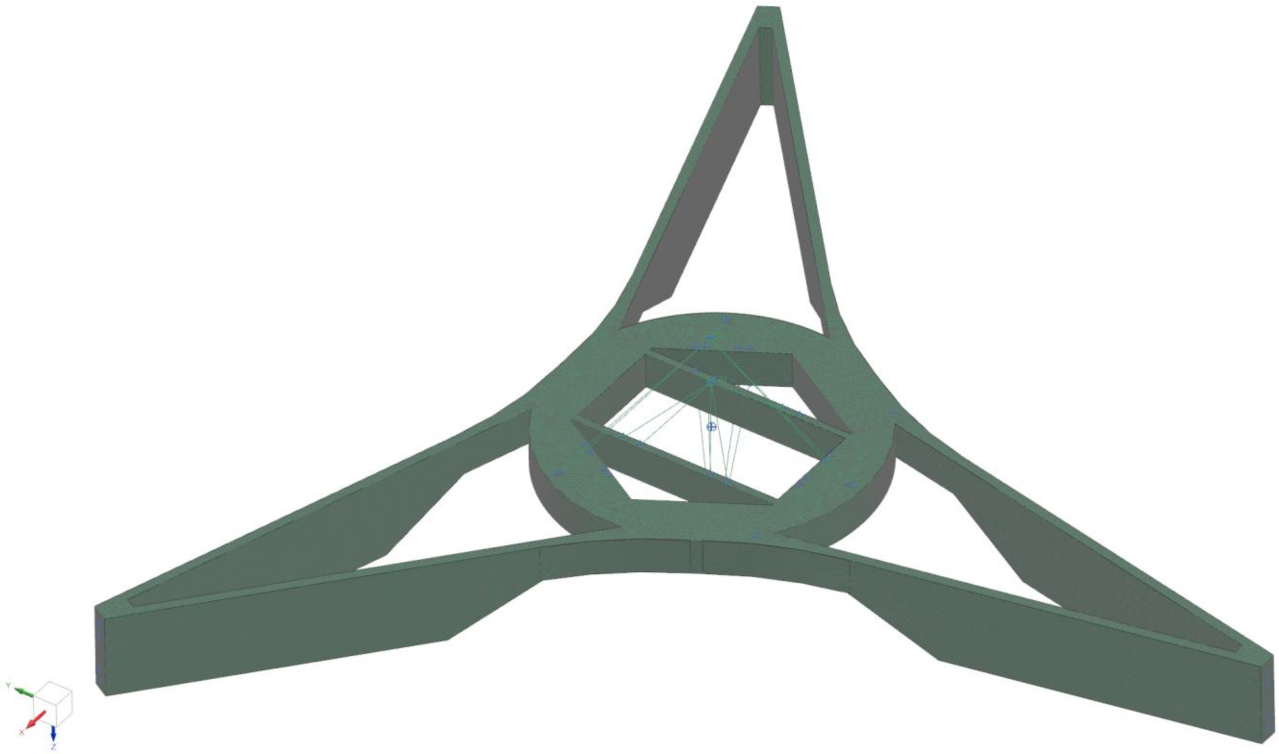

Figure 9. FEM of final design, including 0D meshes and solid 3D shell.

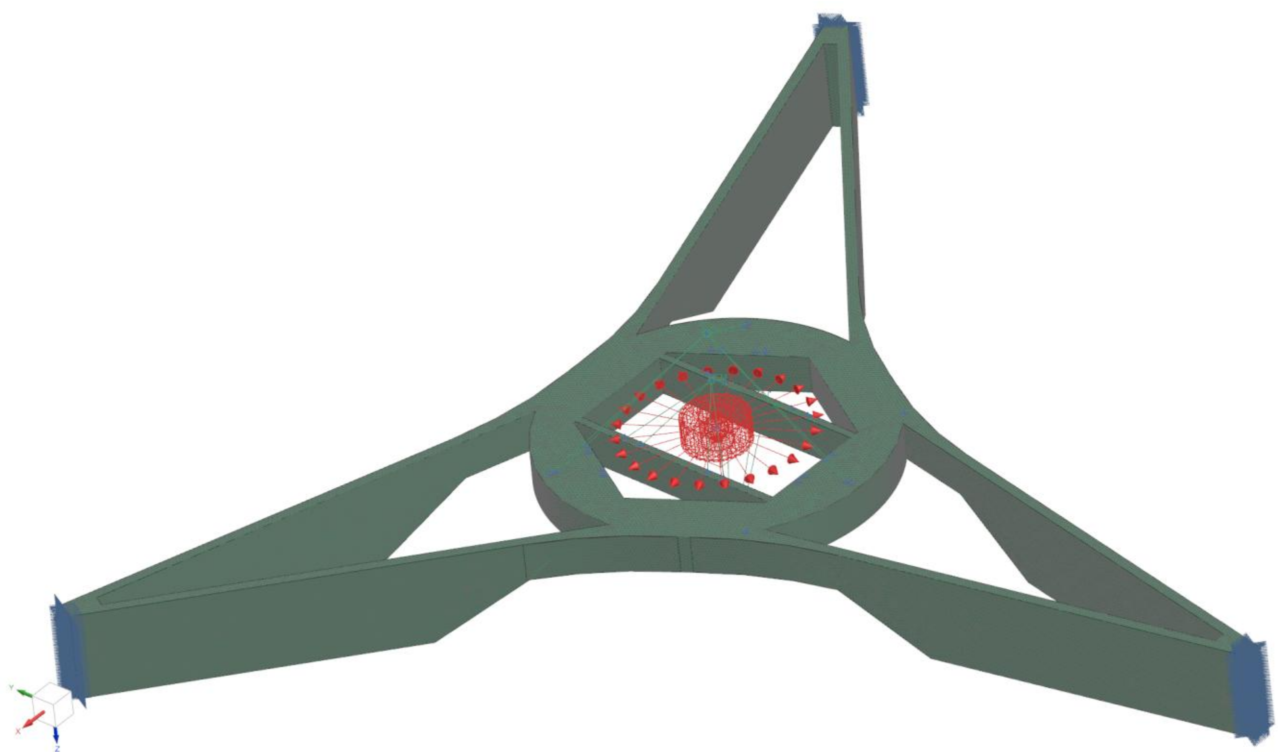

Figure 10. Simulated model of final design including constraints and applied G-loads.

1	T-Low Ultimate MS	margin_of_safety	0DegLow	1.0876
2	T-Low Ultimate MS	margin_of_safety	105DegLow	1.0183
3	T-Low Ultimate MS	margin_of_safety	120DegLow	1.0347

0	T-High Ultimate MS	margin_of_safety	210DegHigh	1.0712
1	T-High Ultimate MS	margin_of_safety	225DegHigh	1.0682
2	T-High Ultimate MS	margin_of_safety	240DegHigh	1.0743

T-Low Yield MS	margin_of_safety	0DegLow	0.5332
T-Low Yield MS	margin_of_safety	105DegLow	0.4823
T-Low Yield MS	margin_of_safety	120DegLow	0.4943

T-High Yield MS	margin_of_safety	210DegHigh	0.5094
T-High Yield MS	margin_of_safety	225DegHigh	0.5072
T-High Yield MS	margin_of_safety	240DegHigh	0.5116

11	T-Low Yield MS	margin_of_safety	225DegLow	-0.5994
12	T-Low Yield MS	margin_of_safety	240DegLow	-0.5998
13	T-Low Yield MS	margin_of_safety	255DegLow	-0.5990

Figure 11. Final design Margins of Safety values and their corresponding loads taken from NX. For the first four and from left to right, Low Temperature Ultimate MS = 1.0183, High Temperature Ultimate MS = 1.0682, Low Temperature Yield MS = 0.4823, High Temperature Yield MS = 0.5072. The final result is the lowest MS but including the lattice when reporting results. This value is – 0.5998.

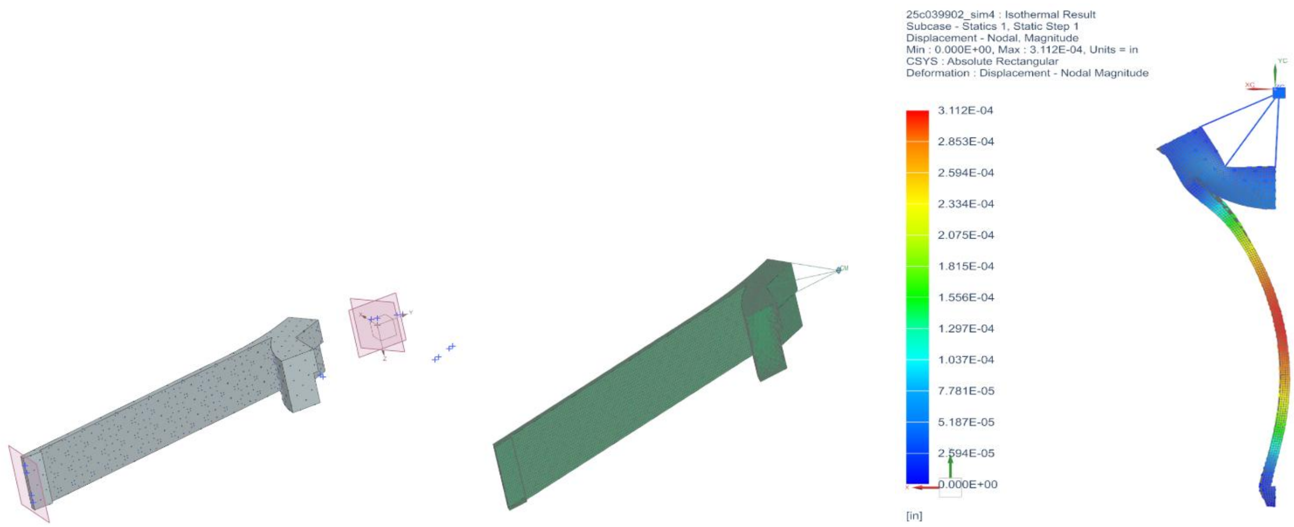

Figure 12. 1/6th model, FEM and simulation verification result. The maximum displacement of the 0D mesh in the center was 3.122E-04 inches.

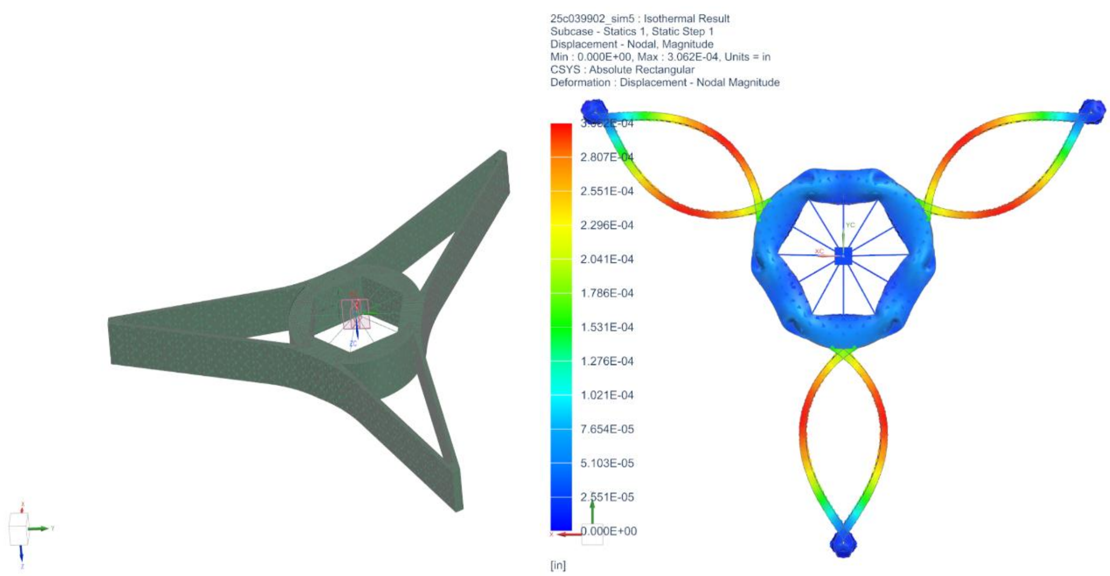

Figure 13. Radially mirrored 1/6th model, FEM and simulation verification result. Maximum displacement of the 0D mesh was 3.062E-04 inches.

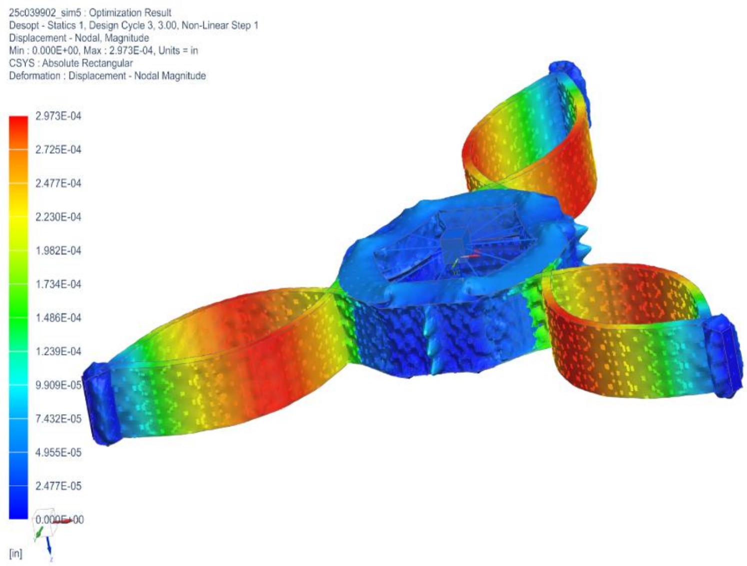

A	B
$gmax	5.00E-03
$	
Cycle	Design Objective
	Value
INITIAL	1.24E-01
1	9.41E-02
2	7.04E-02
3	7.04E-02

DVID	10	11
Label	RODTHICK	SHLTHICK
INITIAL	5.00E-02	1.00E-01
1	4.00E-02	5.00E-02
2	3.00E-02	1.00E-02
3	3.00E-02	1.00E-02
End of Data		

Figure 14. Isothermal Optimization results. This is for the mirrored version of the 1/6th part. The first table shows the weight reducing while the second shows the rod and shell thicknesses reducing.

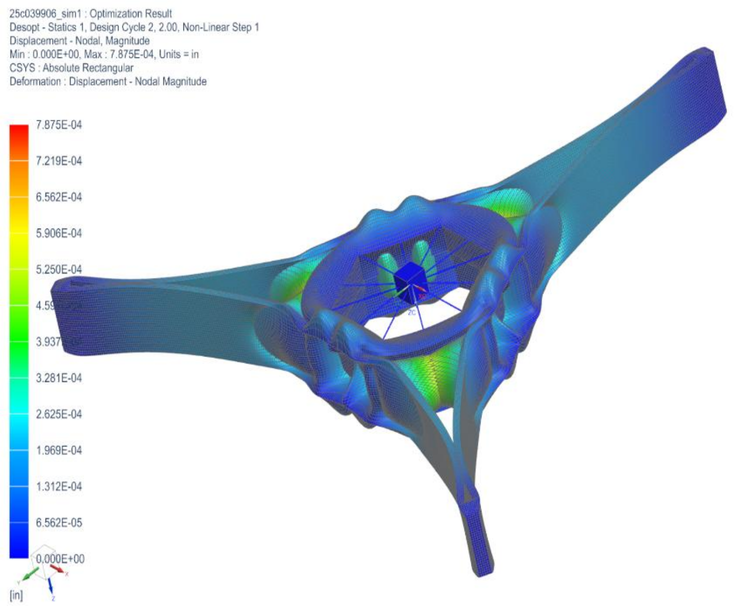

$gmax	5.00E-03
$	
Cycle	Design Ob
	Valu
INITIAL	1.13E-01
1	6.49E-02
2	6.49E-02

DVID	11
Label	SHLTHICK
INITIAL	1.00E-01
1	1.00E-02
2	1.00E-02
End of Data	

Figure 15. Isothermal Optimization results with no lattice. As in Figure 12, the design reduces the variable (shell thickness) to its minimum allowed value.

50	45	1.11E-01	16	-4.(
51	46	1.11E-01	16	-4.(
52	47	1.10E-01	16	-4.(
53	48	1.10E-01	16	-4.(
54	49	1.10E-01	16	-4.(
55	50	1.10E-01	16	-4.(
56				
57	DVID	10	11	
58	Label	RODTHICK	SHLTHICK	

102	43	4.50E-02	7.99E-02
103	44	4.50E-02	7.94E-02
104	45	4.50E-02	7.90E-02
105	46	4.50E-02	7.85E-02
106	47	4.50E-02	7.80E-02
107	48	4.50E-02	7.75E-02
108	49	4.50E-02	7.70E-02
109	50	4.50E-02	7.65E-02
110	End of Data		

Figure 16. Results from final shell and lattice thickness optimization. The shell thickness was reduced and the lattice thickness was reduced to the printable minimum.

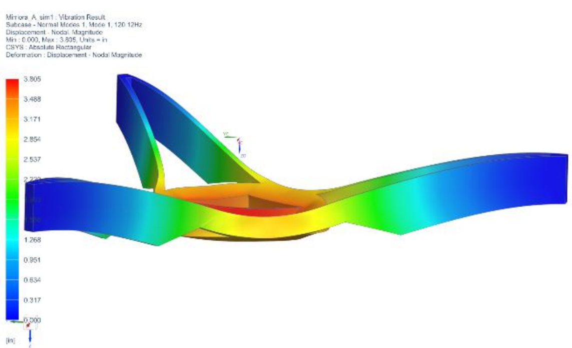

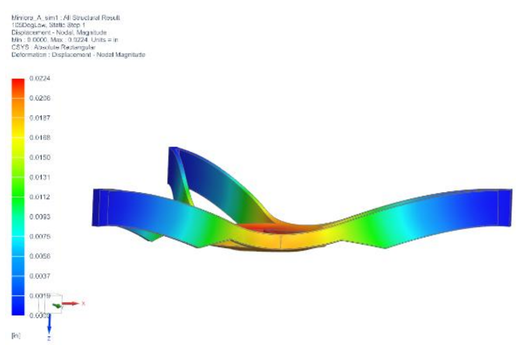

Figure 17. This shows the displacement from the lowest Margin of Safety and the 1st mode of vibration. The latter is on the left while the former is on the right.

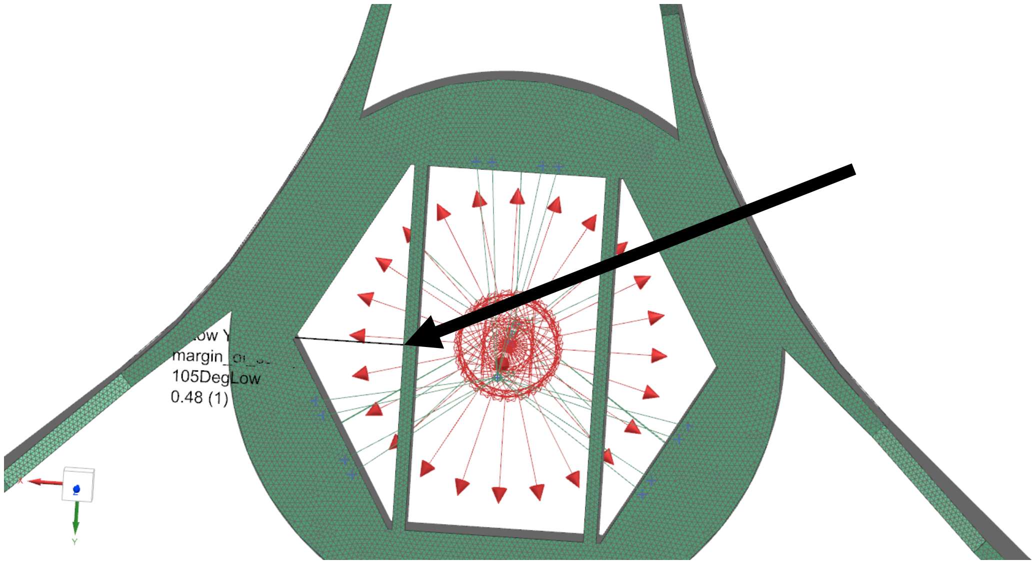

Figure 18. This figure shows the location of the lowest margin of safety no matter which MS was being calculated and whether or not a lattice was included.

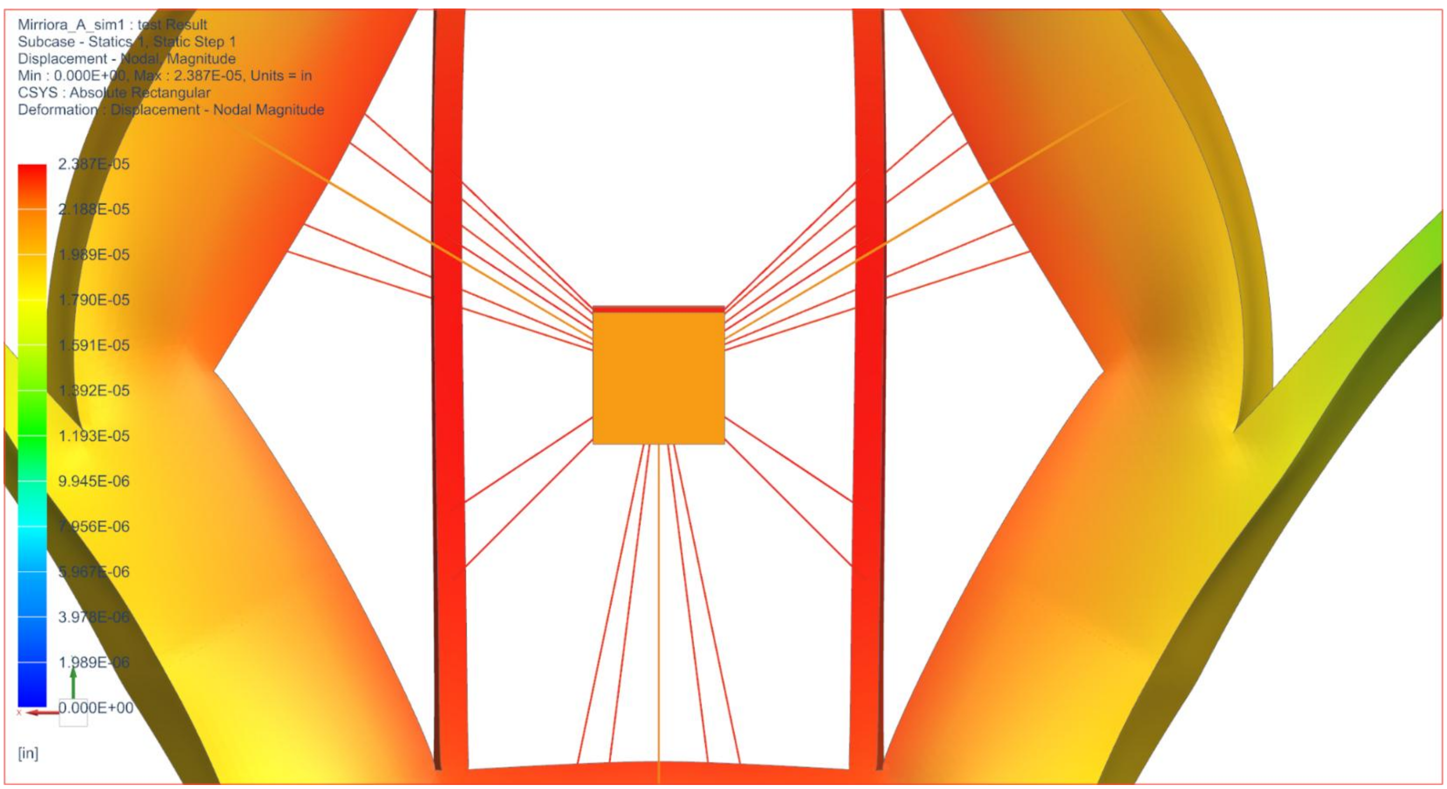

Figure 19. This figure attempts to show the comparison of the displacement of the three concentrated masses under the isothermal load. On The square in the middle, a small red rectangle can be seen just above it, representing the mirror displacing away from the other parts and the center of the structure.

Equal Inner Thickness Mass = 17.3316 lbm

X (in)	Y (in)	Translation (in)	Translation Limit	X (degrees)	Y (degrees)	Rotation (radians)	Rotation Limit
-1.355e-7	5.827e-6	5.828e-6	6.6e-7	-1.545e-5	-1.395e-6	2.707e-7	3.7e-8

Thickness + Perpendicular Beams Mass = 17.70197 lbm

X (in)	Y (in)	Translation (in)	Translation Limit	X (degrees)	Y (degrees)	Rotation (radians)	Rotation Limit
-4.37e-8	5.158e-6	5.158e-6	6.6e-7	-9.5e-6	-4.164e-7	1.659e-7	3.7e-8

Remove Thickness + 2 Angled Beams Mass = 17.35347 lbm

X (in)	Y (in)	Translation (in)	Translation Limit	X (degrees)	Y (degrees)	Rotation (radians)	Rotation Limit
7.825e-7	8.093e-6	8.13e-6	6.6e-7	-3.037e-5	5.968e-6	5.4e-7	3.7e-8

2 Angled Beams - Center Beam Mass = 16.96233 lbm

X (in)	Y (in)	Translation (in)	Translation Limit	X (degrees)	Y (degrees)	Rotation (radians)	Rotation Limit
8.156e-7	-4.93e-6	4.99e-6	6.6e-7	2.372e-5	6.398e-6	4.288e-7	3.7e-8

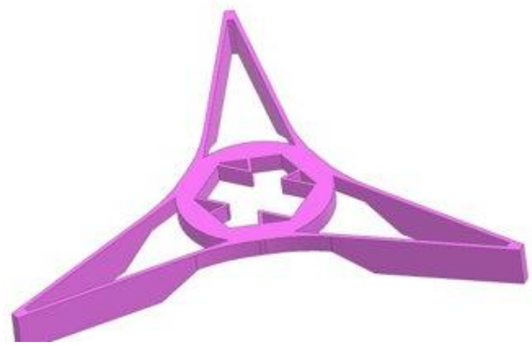

2 Angled Beams - End Beam Mass = 16.96233 lbm

X (in)	Y (in)	Translation (in)	Translation Limit	X (degrees)	Y (degrees)	Rotation (radians)	Rotation Limit
8.602e-7	2.708e-6	2.841e-6	6.6e-7	-1.374e-5	6.55e-6	2.657e-7	3.7e-8

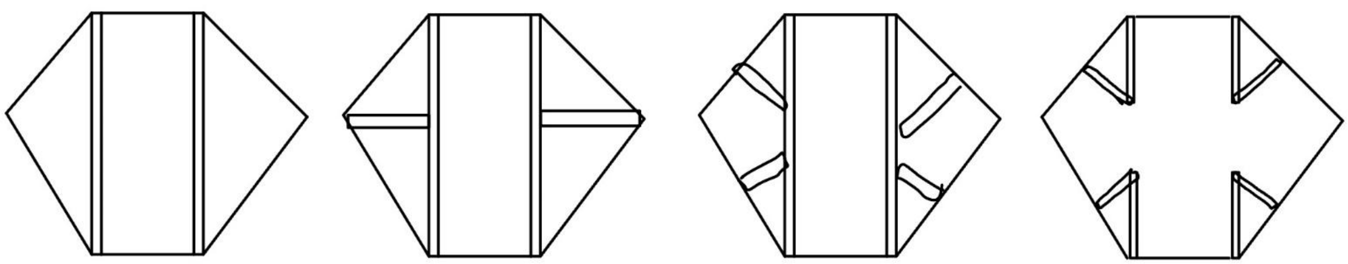

Figure 20. This figure shows the final attempt at changing the actuator mount geometry as well as sketches of previous iterations. It also shows the full tabulated results and the mass of each iteration. From left to right, the first sketch shows the original, the next one adds two perpendicular beams of the same thickness as the original beams. The third replaces those with four angles beams, one perpendicular to each of the four faces. The final sketch removes space in the middle of the two original beams.

					Rank by			
	Calculation	Failure Mode	Load Case	Margin of Safety	Global	Calculation	Failure Mode	Load Case
1	Stress allowable	margin_of_safety	worst-low	0.7672	1	1	1	1
2	Stress allowable	margin_of_safety	worst_high	1.0196	2	2	2	1

	Calculation	Failure Mode	Load Case	Margin of Safety	Global	Calculation	Failure Mode	Load Case
1	Stress allowable	margin_of_safety	worst-low	0.7739	1	1	1	1
2	Stress allowable	margin_of_safety	worst_high	1.0277	2	2	2	1

Figure 21. MS calculations. The top has no lattice and a value of 0.7672 while the bottom does and has a value of 0.7739.

APPENDIX D – INTELLECTUAL PROPERTY

Figure 1. Capstone Project Design for 2024 L3Harris Team.

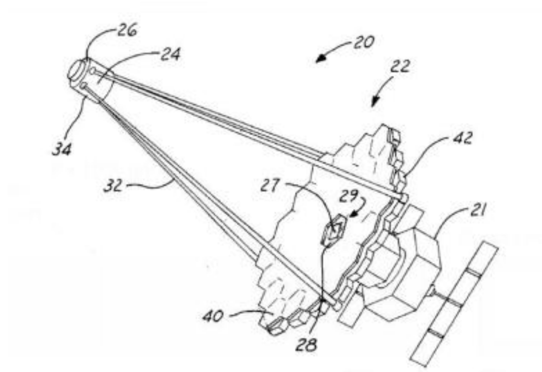

Figure 2. Patented Design by the Boeing Company (US 20050088734A1) [3].

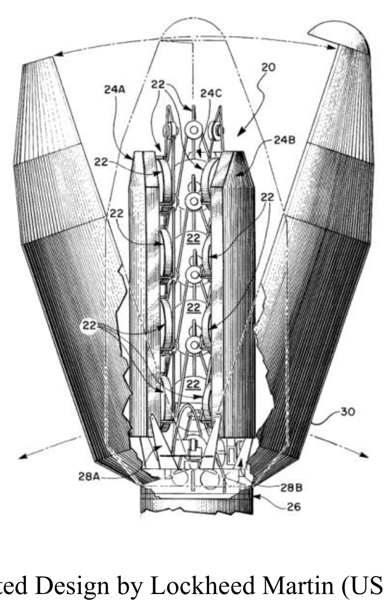

Figure 3. Patented Design by Lockheed Martin (US 005905591A) [4].